nature communications

Article

https://doi.org/10.1038/s41467-025-62890-9

Branched-chain amino acids contribute to diabetic kidney disease progression via PKM2-mediated podocyte metabolic reprogramming and apoptosis

Received: 18 July 2024

Accepted: 1 August 2025

Published online: 25 August 2025

Check for updates

Huishou Zhao[1,7], Dan Sun[2,7], Shan Wang[1,7], Yi Liu[1,7], Xiaojuan Zhao[1], Wenqi Tian[1], Xiuhong Dou[1], Jilong Liu[1], Jinyang Xu[1], Lu Peng[1], Shiren Sun[3], Yunlong Xia[1], Xiaoming Xu[1], Cheng Wang[4], Di Wang[3], Guohong Zhao[5], Xin Wang[5], Huanze Weng[1], Fengyue Ding[1], Pingping Xing[1], Fuyang Zhang[1], Shiyu Liu[6], Wenjun Yan[1] ✉ & Ling Tao[1] ✉

Approximately 30-40% of patients with diabetes develop diabetic kidney disease (DKD). Identifying decisive factors for DKD initiation is crucial. Here, we observed that glomerular podocytes in male and female patients with DKD and db/db mice specifically displayed BCAA catabolic defects. Podocyte-specific PP2Cm (a key BCAA catabolism enzyme) knockout or exogenous BCAA supplementation induced DKD phenotypes including podocyte dysfunction/apoptosis, glomerular pathology, and proteinuria in high-fat (HF)-diet-fed male mice. Mechanistically, BCAAs promoted PKM2 depolymerization and inactivation in podocytes. Depolymerized PKM2 suppressed glucose oxidative phosphorylation (OXPHOS), diverting glucose metabolism towards serine biosynthesis and folate metabolism. Depolymerized PKM2 is also co-transported with DDIT3 into the nucleus, acting as a co-transcriptional factor to enhance DDIT3 transcriptional activity, which promotes Chac1 and Trib3 expression and directly inducing podocyte apoptosis. Thus, BCAA catabolic defects may be one of the missing factors that determine DKD initiation. Targeting BCAA catabolism or PKM2 activation is a promising DKD prevention strategy.

Diabetic kidney disease (DKD) accounts for 30-50% of end-stage renal disease (ESRD) cases[1]. Despite recent treatment advances, only a limited reduction in rates of ESRD from DKD has been observed. New effective therapeutic strategies for preventing DKD initiation and progression are urgently needed.

There is considerable variation in the progression and severity of DKD. Some patients experience a relatively rapid decline in renal function, whilst others maintain normal renal function despite decades of diabetes[2]. The factors influencing this variation in outcome including genetics[3], epigenetics[4,5], and metabolic factors[6,7]. Both glomerular

[1]Department of Cardiology, Xijing Hospital, Fourth Military Medical University, Xi'an, China. [2]Department of Gynecology and Obstetrics, Tangdu Hospital, Fourth Military Medical University, Xi'an, China. [3]Department of Nephrology, Xijing Hospital, Fourth Military Medical University, Xi'an, China. [4]Department of Endocrinology, Xijing Hospital, Fourth Military Medical University, Xi'an, China. [5]Department of Endocrinology, Tangdu Hospital, Fourth Military Medical University, Xi'an, China. [6]State Key Laboratory of Military Stomatology & National Clinical Research Center for Oral Diseases & Shaanxi International Joint Research Center for Oral Diseases, Center for Tissue Engineering, School of Stomatology, Fourth Military Medical University, Xi'an, PR China. [7]These authors contributed equally: Huishou Zhao, Dan Sun, Shan Wang, Yi Liu. ✉e-mail: yanyan517032@163.com; lingtaofmmu@qq.com

and proximal tubular abnormalities contribute to the progression of DKD[6,8,9]. Typical DKD appears in type 1 diabetes mellitus (T1DM) patients 5-15 years after the onset of diabetes. However, only 15-25% of T1DM patients or 30-40% of type 2 diabetes mellitus (T2DM) patients develop DKD. In a longitudinal study, the Joslin Medalist Study of more than 1000 individuals with T1DM for more than 50 years revealed that only some of these patients had developed DKD[10,11]. Individuals who are protected from the development of DKD display only mild renal pathology, despite >50 years of diabetes. These findings indicate that there must be endogenous key pathogenic factors that determine the initiation of DKD. Given the limited contributions of traditional risk factors for CKD, such as hyperglycemia and hyperlipidemia, new metabolic risk factors are more likely to be "decisive factors" for DKD initiation.

Branched chain amino acids (BCAAs, including leucine, isoleucine, and valine) are a group of essential amino acids that account for 15-25% of total dietary protein intake[12]. Data from our laboratory and other laboratories have demonstrated that BCAAs are causally associated with the development of diabetes-associated complications or organ injury[13–16]. In a prospective, observational study, urinary BCAA levels were shown to predict the risk of future DKD progression in T1DM patients[17]. Metabolomic data showed that plasma BCAA- and renal BCAA-derived C3 and C5 acylcarnitines significantly accumulate in Akita-Renin Tg-induced DKD model mice[18]. These findings suggest the potential role of BCAAs in DKD initiation or progression.

DKD is often considered a microvascular complication of diabetes[19], but increasing evidence suggests that podocyte loss and dysfunction are more relevant. Podocytes are highly differentiated postmitotic cells that cannot be readily replaced and may be the "weakest link" in DKD development[20]. Clinical data show that podocyte dysfunction and loss occur early in DKD[21], and the number of podocytes is strongly correlated with proteinuria and appears to be one of the best predictors of DKD[22]. Greater than 20% podocyte loss in animal models causes irreversible glomerular damage, albuminuria, glomerulosclerosis, and subsequent progression to ESRD[23,24]. As highly specialized epithelial cells, podocytes require high energy levels to maintain normal glomerular function. Therefore, maintaining energetic metabolic homeostasis is crucial for the physiological function of podocytes.

In this study, we collected kidney and urine samples from T2DM patients with or without DKD to investigate the key enzymes involved in BCAA catabolism and the overall profile of metabolic alterations. Intriguingly, we found that podocytes in glomeruli from both male and female patients with DKD specifically exhibited BCAA catabolic defects, which were also observed in podocytes of db/db mice. Wild-type mice fed a 16-week high-fat (HF) diet did not exhibit notable DKD renal injury[25]. However, endogenous BCAA catabolic defects by podocyte-specific protein phosphatase protein phosphatase-2C (PP2Cm) deletion or exogenous supplementation with BCAAs induced significant DKD phenotypes in male mice after 16 weeks of a HF diet. Mechanistically, BCAA-induced podocyte metabolic reprogramming manifests as inhibited glucose oxidation, increased a shift of glucose catabolism to serine biosynthesis and folate metabolism. The urine and kidney samples of patients with DKD support the finding that BCAA catabolic defects promote serine biosynthesis and folate metabolism in animal podocytes. BCAA-induced podocyte metabolic reprogramming was mediated by the enzymatic inactivation of PKM2. Using podocyte-specific PKM2-deleted mice and primary podocytes with PKM2 knockout or overexpression, we showed that the nonenzymatic cotranscriptional activity of PKM2 leads to podocyte apoptosis. Both the enzymatic inactivation and nonenzymatic cotranscriptional activity of PKM2 contribute to the progression of DKD. Our results provide evidence that BCAA catabolic defect in podocytes is a possible missing factor that determining DKD initiation. Targeting PKM2 or BCAA catabolism may be a promising strategy for DKD prevention and treatment.

Results

Glomerular podocytes display BCAA catabolic defects in patients with DKD and db/db mice

The BCAA catabolic pathway includes general BCAA oxidation, leucine oxidation, and isoleucine/valine oxidation. After general BCAA oxidation, BCAAs are catabolized to isobutyryl-CoA, α-methylbutyryl-CoA, or isovalery-CoA. These three intermediate metabolites then enter the leucine oxidation pathway or isoleucine/valine oxidation pathway to produce acetyl-CoA, propionyl-CoA, or succinyl-CoA, which then enters the tricarboxylic acid (TCA) cycle. The enzymes involved in general BCAA oxidation mainly include PP2Cm, branched-chain α-keto acid dehydrogenase kinase (BDK) and the rate-limiting branched-chain α-keto acid dehydrogenase complex (BCKD), which consists of BCKDHA, BCKDHB, dihydrolipoamide branched chain transacylase E2 (DBT) and dihydrolipoamide dehydrogenase (DLD). BDK phosphorylation of BCKDHA E1α at Ser 293 [P-BCKDE1α (Ser 293)] leads to BCKD inactivation, while PP2Cm dephosphorylates BCKDHA E1α at Ser 293, resulting in BCKD activation[26,27]. Other general BCAA oxidative pathways include BCAA transaminase 1/2 (BCAT1/2). Analysis of proteomic data from isolated glomeruli from patients with DKD or non-DKD patients with an extreme duration of diabetes (≥50 years, the Joslin Medalist Study)[28], we found that enzymes involved in general BCAA oxidation, leucine oxidation, or isoleucine/valine oxidation have tendency to be downregulated in the DKD group (Table S1). Through nontargeted metabolomics of 24-hour urine samples, we found that the levels of two BCAA catabolites, 4-methyl-2-oxopentanoate and methylmalonic acid, were significantly greater in the urine of male and female patients with early stage of DKD (eGFR >90 ml/min/1.73 m^2, 30≤ urinary albumin/creatinine ratio <70) than in that of non-DKD patients who were diagnosed with T2DM for an average of 15 years (Fig. 1a).

Since glomerular and proximal tubular abnormalities both contribute to the progression of DKD[6,8], we collected renal biopsy samples from non-DKD or patients with DKD by kidney tissue puncture and determined the expression of P-BCKDE1α (Ser 293), PP2Cm, and BDK in glomerular sections and renal proximal tubules, respectively. We found that the P-BCKDE1α (Ser 293) level was significantly increased in the glomeruli of patients with DKD than in those of non-DKD patients (Fig. 1b and Supplementary Fig. 1a), but did not significantly change in proximal tubules (Supplementary Fig. 1b).

To reveal the distribution of P-BCKDE1α (Ser 293) across different cell types in the glomeruli, we conducted periodic acid-Schiff (PAS) and P-BCKDE1α (Ser 293) double staining. As shown in Supplementary Fig. 1c, the cells that highly expressed P-BCKDE1α (Ser 293) were localized to the outside of the basement membrane. P-BCKDE1α (Ser 293) was localized at WT1 (podocyte-specific marker) positive cells in the glomeruli of patients with DKD (Fig. 1c, d). These results showed that podocytes highly expressed P-BCKDE1α (Ser 293) in the glomeruli of patients with DKD. In addition, through double staining of WT1 with PP2Cm or BDK, we found that PP2Cm and BDK expression was significantly lower in podocytes from male and female patients with DKD than in those of non-DKD patients (Fig. 1c, d, Supplementary Fig. 1d, e).

Next, we isolated and purified glomeruli from db/db mice, a model of DKD, via iron (III) oxide perfusion methods. The purity of the glomeruli was greater than 95% (Supplementary Fig. 2a). We performed Western blotting and found that, compared with C57BL/6 mice, both male and female db/db mice exhibited significantly decreased expression of PP2Cm, BDK but increased P-BCKDE1α (Ser 293) to total BCKD expression ratios in glomeruli (Fig. 1e, f). We also performed dual staining for WT1 with P-BCKDE1α (Ser 293) or PP2Cm in kidney sections from db/db mice. Consistent with the results in patients with DKD, podocytes, as indicated by WT1-positive staining in the glomeruli of db/db mice, exhibited substantially decreased PP2Cm and BDK expression and increased P-BCKDE1α (Ser 293) expression. All these changes were not observed in proximal tubules of both male and female db/db mice (Fig. 1g, h, Supplementary Fig. 2b, c). We then

https://doi.org/10.1038/s41467-025-62890-9

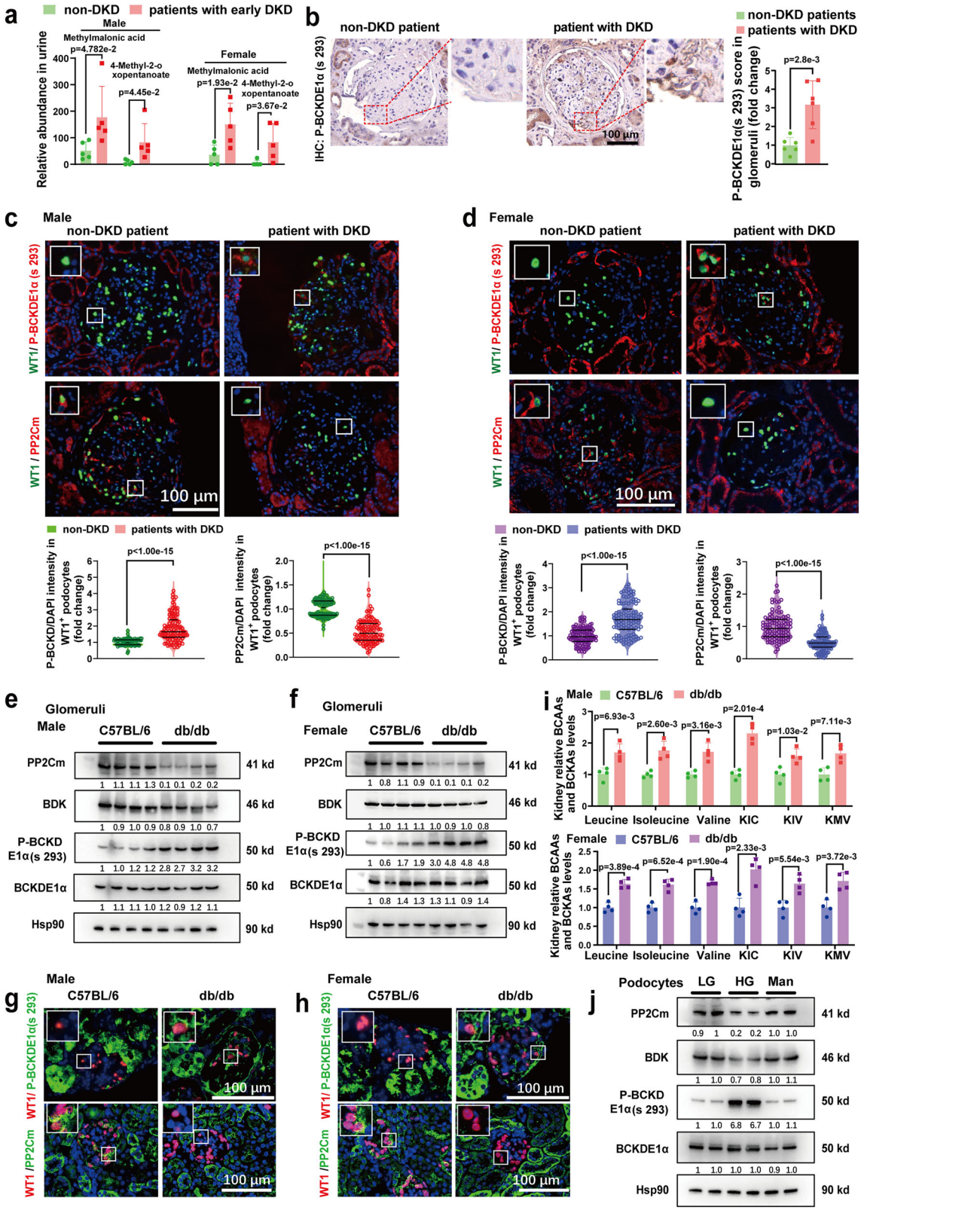

detected the BCAAs and BCKAs levels of isolated glomeruli as previously reported[29]. As shown in Fig. 1i, the glomerular BCAAs and BCKAs levels were also significantly increased in db/db mice than that in C57BL/6 mice. In addition, we exposed primary podocytes or primary proximal tubular cells to high glucose (HG, 25 mM glucose) conditions for 24 h. We found that HG significantly decreased the mRNA and protein levels of PP2Cm while increasing the P-BCKDE1α (Ser 293) to BCKD expression ratio (Fig. 1j, Supplementary Fig. 2e), but did not induce significant change of PP2Cm, BDK, and P-BCKDE1α (Ser 293) in proximal tubular cells (Supplementary Fig, 2d–f). Consistently, human DKD snRNA and scATAC-seq data[30] from the Kidney Interactive Transcriptomics dataset also showed that PP2Cm mRNA expression, and gene activity & accessibility are decreased in the podocytes, but not obviously changed in proximal tubular cell (Supplementary

Fig. 1 | Glomerular podocytes exhibit BCAA catabolic defects in patients with DKD and DKD db/db mice. a The levels of 4-Methyl-2-oxopentanoate and Methylmanic acid in the 24 hrs urine samples were tested by non-targeted metabolomics from male or female T2DM patients without DKD (non-DKD, $n = 5$) or patients with early DKD ($n = 5$). **b** Representative images of immunohistochemistry (IHC) staining of P-BCKDE1α (Ser 293) in glomeruli. The P-BCKDE1α (Ser 293) score was evaluated by IHC in glomerular sections. A total of 70-110 glomeruli from $n = 6$ patients per group were analyzed. **c, d** Upper, representative images of double staining of P-BCKDE1α (Ser 293) and PP2Cm with Wilms tumor-1 (WT-1, a podocyte-specific marker) in kidney sections. Bottom, quantification of P-BCKDE1α (Ser 293) and PP2Cm intensities in WT1 positive podocytes, normalized to DAPI. Male: p-BCKD/DAPI intensities (median (Q1–Q3)) 0.98 (0.86 − 1.15) versus 1.65 (1.32 − 2.35), $n = 107$ cells per group; PP2Cm/DAPI intensities 1.03 (0.87 − 1.16) versus 0.50 (0.35 − 0.69), $n = 108$ cells per group. Female: p-BCKD/DAPI intensities 0.96 (0.77 −1.24) versus 1.67 (1.27 −2.10), $n = 107$ cells per group; PP2Cm/DAPI intensities 0.94 (0.69 −1.22) versus 0.49 (0.38 −0.67), $n = 107$ cells per group. White boxes indicate the localization of WT1 with P-BCKDE1α or PP2Cm. **e, f** Representative Western blots of PP2Cm, P-BCKDE1α and BDK were detected in female and male C57BL/6 mice or db/db mice. $n = 4$ mice per group. **g, h** Representative double-staining images of PP2Cm, P-BCKDE1α (Ser 293) with WT1. $n = 4$ mice per group. **i** The concentration of BCAAs (including leucine, isoleucine and valine) or BCKAs (including KIC, KIV, KMV) were measured in isolated glomeruli, $n = 4$ per group. **j** Representative Western blots of BDK, PP2Cm, P-BCKDE1α (Ser 293) and total BCKDE1α in primary podocytes under low-glucose (LG, 5.5 mM glucose) or high-glucose (HG, 25 mM glucose) conditions for 24 hrs. 20 mM mannitol (Man) plus 5 mM glucose were treated as the osmotic control group, $n = 4$ total samples per group. The data were presented as the mean ± SD and were analyzed by unpaired two-tailed Student's t test.

Fig. 2g–h). These results suggested that podocyte is susceptible to developing BCAAs catabolism under DKD condition. Therefore, we demonstrated that glomerular podocytes in male and female patients with DKD and db/db mice exhibit BCAA catabolic defects.

BCAA catabolic defects exacerbated HF diet-induced renal injury in mice

To elucidate the causal relationship between podocyte BCAA catabolic defects and DKD progression, we constructed podocyte-specific PP2Cm knockout mice ($PP2Cm^{f/f}$ Cre^{+}, a BCAA catabolic defect mouse model) using Nphs2-Cre^{+} mice crossbred with $PP2Cm^{f/f}$ mice (Supplementary Fig. 3a, b). PP2Cm protein expression was significantly decreased in the isolated glomeruli of the $PP2Cm^{f/f}$ Cre^{+} mice, as evidenced by Western blotting (Supplementary Fig. 3c). Podocyte-specific PP2Cm knockout did not display BCAAs accumulation and significant renal injury as indicated by moderately increased plasma creatinine, urinary nitrogen, and urinary microalbumin levels (Supplementary Fig. 3d–h). $PP2Cm^{f/f}$ Cre^{+} mice and their wild-type littermates ($PP2Cm^{f/f}$) were then fed an HF diet for 16 weeks. As shown in Supplementary Fig. 3i–m, podocyte-specific PP2Cm knockout did not affect body weight, fasting plasma BCAA levels, glucose concentrations, or glucose/insulin tolerance.

DKD is associated with pathological glomerular changes, including glomerular hypertrophy, mesangial expansion, lipid accumulation, and glomerular basement membrane thickening[6,31]. We found that podocyte-specific PP2Cm knockout significantly increased the kidney weight-to-body weight ratio (Fig. 2a), mesangial matrix expansion, and renal lipid droplets accumulation as indicated by TG measurements and Oil red O staining (Fig. 2b–d), but did not affect lipid β-oxidation in proximal tubules (Supplementary Fig. 3n). Consistently, transmission electron microscopy (TEM) analysis revealed that podocyte-specific PP2Cm knockout promoted foot process fusion and significantly increased thickening of the basal membrane (Fig. 2e). Compared with the HF-fed $PP2Cm^{f/f}$ mice, the HF-fed $PP2Cm^{f/f}$ Cre^{+} mice also exhibited a significantly decreased number of podocytes but significantly increased glomerular cell apoptosis (Fig. 2f, g) and significantly decreased mRNA and protein expression of podocyte-specific markers, such as Nephrin, Nphs2, P-cadherin, and Synaptopodin (Synpo) (Fig. 2h–j). In addition, we found that the HF-fed $PP2Cm^{f/f}$ Cre^{+} mice exhibited a significantly increased urinary albumin-to-creatinine ratio (Fig. 2k). In vitro, BCAAs directly induced downregulation of Synpo and Nphs2 protein levels in primary podocytes (Fig. 2l). These results suggest that podocyte-specific BCAA catabolic defects lead to podocyte injury and apoptosis and result in renal damage in HF-fed obese mice.

Furthermore, we exogenously supplemented BCAA to HF diet-fed mice, a BCAA overload mouse model. BCAA supplementation has been reported to inhibit caloric intake[32], and caloric intake contributes to development of DKD[33]; thus, we divided mice into 3 groups: HF (HF diet with drinking water containing 4% amino acids), HF/Paired (HF diet with drinking water containing 4% amino acids, food intake matched with HF/BCAAs), and HF/BCAA (HF diet with drinking water containing 4% BCAAs). As expected, the body weight gain and food intake of the HF/BCAA group were comparable to those of the HF/Paired group (Supplementary Fig. 4a, b). BCAA supplementation significantly increased plasma BCAA levels (Supplementary Fig. 4c), increased the kidney weight-to-body weight ratio (Supplementary Fig. 4d), and increased mesangial matrix expansion and cast formation (Supplementary Fig. 4e, f). Moreover, BCAA overload significantly increased renal lipid droplets accumulation, as indicated by oil red O staining, TG measurement and TEM analysis (Supplementary Fig. 4g, h), but did not affect lipid β-oxidation in proximal tubules (Supplementary Fig. 4i). TEM analysis revealed substantial lipid droplets accumulation in the brush borders of proximal tubular epithelial cells (Supplementary Fig. 4g), which substantiated the leakage of blood lipids from the renal filtration membrane barrier to the tubule lumen and their reabsorption by renal proximal tubular cells. TEM also showed that BCAA supplementation significantly exacerbated HF-induced GBM thickening and foot process fusion (Supplementary Fig. 4j). BCAA supplementation significantly decreased the number of podocytes but significantly increased podocyte apoptosis in the HF/BCAA mice (Supplementary Fig. 4k, l). In addition, BCAA accumulation significantly decreased the mRNA and protein expression levels of the podocyte markers Nephrin, Nphs2, P-cadherin, and Synpo (Supplementary Fig. 4m–o). Moreover, we found that BCAA supplementation significantly increased urinary albumin/creatinine levels (Supplementary Fig. 4p) compared to those in the HF/Paired group. Overall, we confirmed that BCAA catabolic defects and overload contribute to DKD progression by inducing podocyte injury and loss.

BCAA-induced podocyte metabolic reprogramming manifests as inhibited glucose oxidation, promoted a shift of glucose catabolism to serine biosynthesis and folate metabolism

To clarify the mechanism underlying BCAA-induced podocyte dysfunction and death, we used RNA sequencing to analyze the transcriptomic profiles of differentiated MPC-5 podocytes exposed to HG or HG/BCAAs. As shown in Fig. 3a, Gene Ontology analysis revealed that the top 7 downregulated pathways (shown in green) in the HG/BCAA group were regulation of locomotion, cellular component movement, motility, migration, epithelial cell differentiation, actin skeleton, and skeleton organization. Indeed, BCAA supplementation significantly downregulated the expression of skeletal genes such as *Tubb2b*, *Tuba4a*, and *Tuba1a* and the metalloproteinase genes *Adamts1, Thbs1* and *Sema3c* both in vitro and in vivo (Fig. 3b). Consistent with the alterations in the expression of these genes, F-actin immunofluorescence showed worse actin cytoskeleton rearrangement in HG/BCAA-treated podocytes than in HG-treated podocytes (Fig. 3c). Interestingly, the top 7 upregulated metabolic pathways (shown in red) in the HG/BCAA group included cofactor metabolic process, ncRNA

https://doi.org/10.1038/s41467-025-62890-9

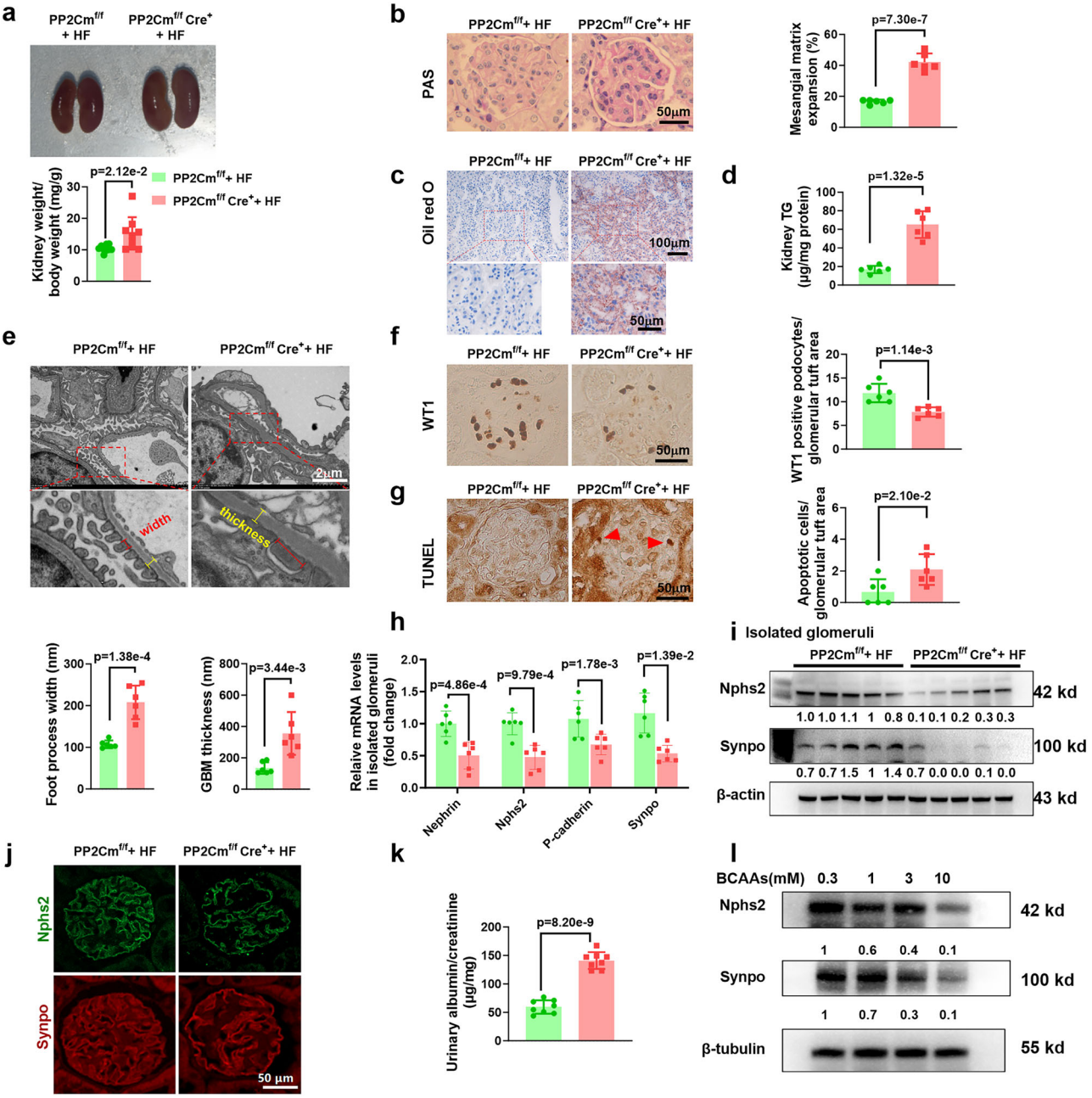

Fig. 2 | BCAA catabolic defects exacerbated HF diet-induced diabetic renal injury. a Kidney weight-to-body weight ratios, $n = 9$. **b** Left, representative images of PAS-stained kidney sections; right, measurements of mesangial matrix expansion (an average of 42 glomeruli was assessed), $n = 6$ per group. **c** Representative images of oil red O staining of kidney sections from PP2Cm$^{f/f}$ Cre^{+} +HF and PP2Cm$^{f/f}$ + HF mice. $n = 6$. **d** Renal tissue triglyceride (TG) levels, $n = 6$. **e** Representative transmission electron microscopy (TEM) images of glomerular podocytes and measurements of foot process width and glomerular filtration barrier (GBM) thickness. An average of 100 measurements were performed for each mouse, $n = 6$ mice per group. **f** Representative immunostaining images of glomerular sections and quantification of WT1-positive podocytes in mice in the PP2Cm$^{f/f}$ Cre^{+} +HF and PP2Cm$^{f/f}$ + HF groups. WT-1-positive cell number was normalized to glomerular tuft area. In each group, 60-91 glomeruli from 6 mice were evaluated. **g** TUNEL staining and quantification of TUNEL-positive nuclei in glomeruli. TUNEL positive cell was normalized to glomerular tuft area. A total of 61-95 glomeruli from 6 mice per group were evaluated. **h** The mRNA expression of *Nephrin*, *Nphs2*, *P-cadherin*, and *Synaptopodin (Synpo)*, $n = 6$. **i** Measurement of Nphs2 and Synpo protein expression in the isolated glomeruli by Western blotting, $n = 5$ mice per group. **j** Measurements of Nphs2 (green) and Synpo (red) expression in glomerular sections by immunostaining, $n = 5$ mice per group. **k** Urinary albumin was measured and was presented as the ratio of urinary albumin/creatinine, $n = 8$. **l** Representative Western blots of Nphs2 and Synpo in primary podocytes that exposed to indicated concentration of BCAAs for 24 hrs. $n = 3$, per group. The data were presented as mean ± SD, and analyzed by unpaired two-tailed Student's t test.

metabolic process, nucleoside metabolic process, ribonucleoprotein complex biogenesis, monocarboxylic acid metabolism, and DNA metabolic process (Fig. 3a). A more detailed analysis of the top 7 upregulated metabolic pathways revealed 33 genes (cutoff: fold change ≥ 2; P < 0.05) that showed significantly upregulated expression in the HG/BCAA group (Fig. 3d). Among these genes, 10 were metabolism related genes which expression was significantly upregulated by BCAA supplementation both in vitro and in vivo (Fig. 3e). These 10 genes include 5 metabolic enzymes (Phgdh, Psat1, Psph, Shmt2, Mthfd2) and 2 transporters (Slc1a4 and Slc1a5) that are involved in

https://doi.org/10.1038/s41467-025-62890-9

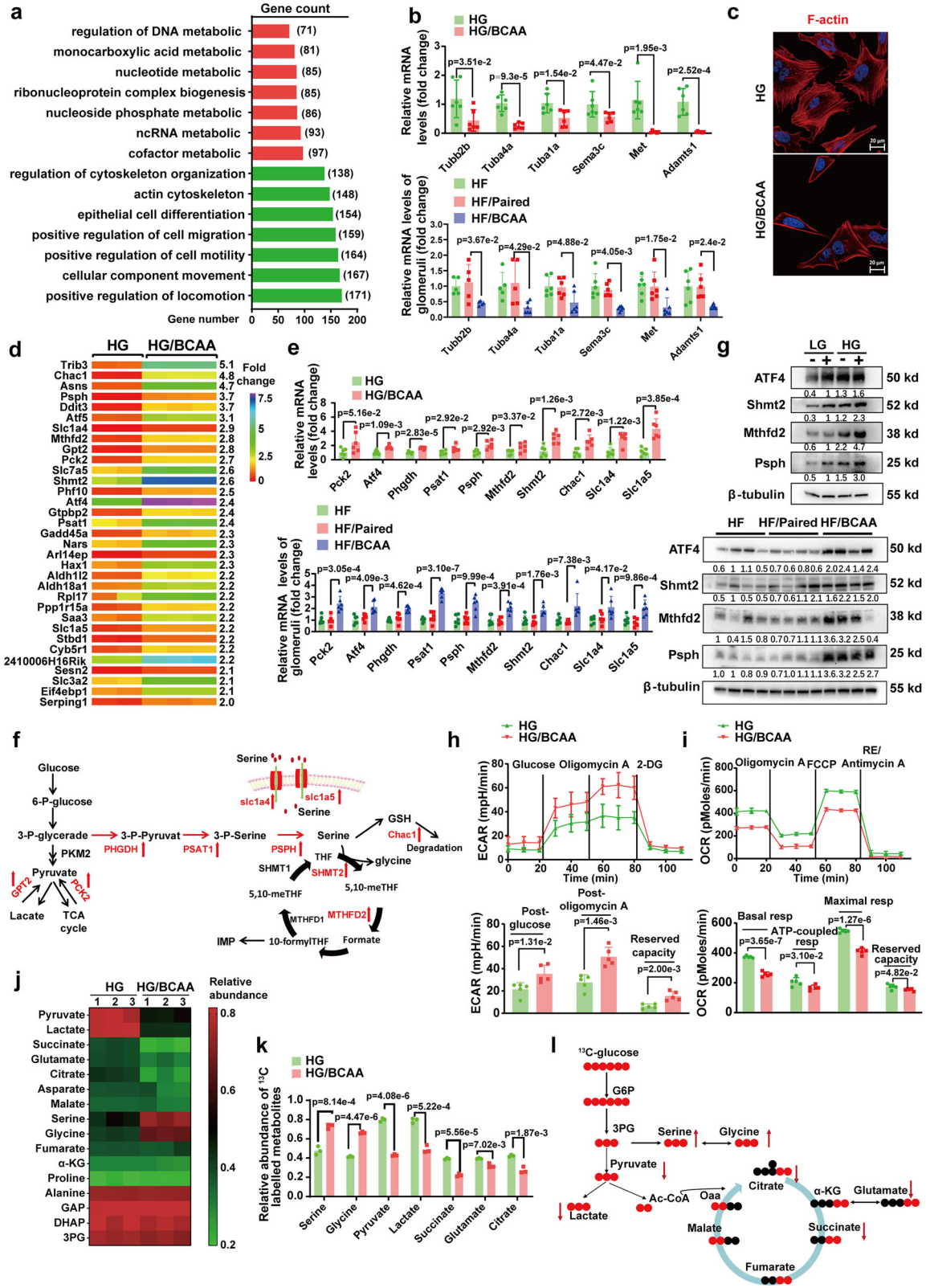

serine biosynthesis and folate metabolism, which suggested that BCAA administration promoted glucose-derived serine biosynthesis and folate metabolism. We graphically show these genes in Fig. 3f. We confirmed that the protein expression levels of Atf4, Psph, Shmt2, and Mthfd2 were also markedly increased in the BCAA-supplemented samples in vitro and in vivo (Fig. 3g). Collectively, these results indicate that BCAA catabolic defects promote serine biosynthesis and folate metabolism in podocytes.

Podocytes are highly specialized epithelial cells that require substantial energy to maintain glomerular integrity and function. To confirm whether BCAA accumulation disrupts podocyte metabolic homeostasis, Seahorse analysis was performed to assess podocyte glucose metabolism. Compared to HG treatment alone, HG/BCAA treatment significantly increased the extracellular acidification rate (ECAR) in primary podocytes after glucose and oligomycin A administration, suggesting that supplementation of BCAAs significantly

Fig. 3 | BCAA-induced metabolic reprogramming in podocyte. a RNA sequencing of differentiated MPC-5 podocytes treated with HG or HG plus 3 mM BCAAs (HG/BCAA) (leucine: isoleucine: valine =1:1:1) for 24 h. We show the top 7 upregulated pathways (red) and the top 7 downregulated pathways (green) using Gene Ontology (GO) and modified Fisher's exact test. **b** The mRNA expression in primary podocytes (upper, $n = 6$) and isolated glomeruli from mice (lower, $n = 5$ mice for Tubb2b in all groups; $n = 5$ mice for Tuba4a in HF and HF/paired groups; $n = 6$ mice for others). **c** Representative immunofluorescence images of F-actin expression in MPC-5 podocytes. **d** Heatmap of the top 33 genes from (**a**) with cutoff of $p < 0.05$ and a fold change ≥ 2 (Mann–Whitney U test). The numbers on the right indicate the fold changes. **e** The mRNA expression in primary podocytes (upper) and isolated glomeruli from mice (lower), $n = 6$. **f** Graphical representation of genes involved in de novo serine biosynthesis and one-carbon metabolism. **g** Representative Western blots of key protein in the serine and folate biosynthetic pathway in both primary podocytes ($n = 4$) and isolated glomeruli from mice ($n = 4$ mice per group). **h** Upper, extracellular acidification rate (ECAR) in cultured primary podocytes; bottom, statistical analyses of post-glucose, post-oligomycin A and reserved capacity in ECAR, $n = 5$. **i** Upper, oxygen consumption rate (OCR) of primary podocytes; bottom, statistical analyses of baseline respiratory capacity, ATP-coupled respiratory capacity, maximum respiratory capacity and reserve respiratory capacity in the OCR. 2-DG, 2-deoxyglucose. FCCP, cyanide-4-(trifluoromethoxy) phenylhydrazone. RE, rotenone. Resp, respiration. $n = 5$. **j** Heatmap of the relative abundance of the carbon-13 (^{13}C)-labeled main metabolites from uniformly carbon-13-labeled glucose ([U-$^{13}C6$] glucose) (25 mM) treated primary podocytes. GAP, glyceraldehyde-3-phosphate; DHAP, dihydroxyacetone phosphate; 3-PG, 3-phosphoglycerate; α-KG, alpha-ketoglutarate. **k** Incorporation of ^{13}C from [U-$^{13}C6$] glucose (25 mM) into the indicated metabolites at 6 h in primary podocytes. $n = 3$. **l** Schematic metabolic map of [U-$^{13}C6$]-labeled glucose metabolism. The data were presented as mean ± SD, and analyzed by unpaired two-tailed Student's t test (**a, b** upper, **d, e** upper, **h, i**, and **k**) or one-way ANOVA (**b** bottom, **e** bottom).

increases post-glucose, post-oligomycin A and the reserved capacity of ECAR in podocytes (Fig. 3h). Oxygen consumption rate (OCR) analysis revealed that BCAA supplementation decreased basal respiration, ATP-coupled oxygen consumption, and the maximal OCR and decreased reserve respiratory capacity (Fig. 3i). BCAA addition increased podocyte ECAR and suppressed glucose OCAR but to a lesser extent under LG conditions (Supplementary Fig. 5a, b). Taken together, these results demonstrate that BCAA addition inhibited OXPHOS activity but promoted glycolysis-derived acids production in podocytes.

To elucidate how BCAA addition affects podocyte glucose metabolic flux, we performed carbon-tracing experiments using uniformly carbon-13-labeled glucose [(U-$^{13}C6$) glucose]. These experiments showed that the addition of 3 mM BCAAs did not affect glucose-derived glyceraldehyde-3-phosphate (GAP), dihydroxyacetone phosphate (DHAP), 3-phosphoglycerate (3-PG), alanine, proline, malate, aspartate, alpha-ketoglutarate (α-KG) or fumarate levels (Supplementary Fig. 5c). However, the addition of BCAAs led to a pronounced increase in serine and glycine biosynthesis rates, as well as serine and glycine pools, in primary podocytes (Fig. 3j–l), and significantly decreased the production of glucose-derived pyruvate, lactate and TCA cycle intermediate metabolites, such as succinate, glutamate, and citrate (Fig. 3j–l). We then detected the folate/folic acids levels in podocytes. As shown in Supplementary Fig. 5d, BCAAs addition significantly increased folate/folic acids production in podocytes. Besides, we found that BCAAs significantly inhibit ATP production by glycolysis in podocytes (Supplementary Fig. 5e). Collectively, these data suggest that BCAAs inhibit glucose OXPHOS but mediate a shift in glucose metabolism to serine biosynthesis and folate metabolism in podocytes.

Serine and folate metabolism were significantly increased in the kidneys of patients with DKD

To determine whether serine biosynthesis and folate metabolism are also increased in kidneys from patients with DKD, we analyzed the urinary metabolic profiles of non-DKD and patients with DKD. A total of 4233 metabolites in the urine were detected on mass spectrometry, including 1285 ion features (positive mode) and 2948 ion features (negative mode). As shown in Fig. 4a, the heatmap showed 430 differentially expressed urinary metabolites between the non-DKD and DKD groups. KEGG pathway enrichment analysis revealed that the folate metabolism pathway and glycine, serine, and threonine metabolism pathways were significantly enriched in patients with DKD (Fig. 4b). Interestingly, folate metabolism was the top enriched pathway and included 7 significantly differentially abundant intermediate metabolites (Fig. 4c, d). Specifically, the abundances of 2 serine biosynthetic metabolites and 6 folate metabolites were significantly increased in the male and female DKD group (Fig. 4e–h). Consistently, immunofluorescence staining revealed that the expression levels of the key enzymes involved in folate metabolism, MTHFD2 and SHMT2, as well as that of the key enzyme involved in serine biosynthesis, PSPH, were significantly increased in the glomeruli of patients with DKD (Fig. 4i–k). More importantly, all these enzymes were found to localize at WT1 positive podocytes. These data from the urine and kidney samples of patients with DKD support the finding that BCAA catabolic defects promote serine biosynthesis and folate metabolism in animal podocytes.

BCAA administration elicited podocyte metabolic reprogramming by inducing PKM2 depolymerization and inactivation

To elucidate the mechanism underlying the BCAA-induced glucose metabolic shift, we determined the expression levels of key glycolytic enzymes in podocytes. BCAA addition significantly upregulated glucokinase (GCK) and pyruvate kinase M2 isoform (PKM2) expression both in vivo and in vitro (Fig. 5a, b, Supplementary Fig. 6a, b) but did not induce significant changes in the protein expression levels of phosphofructokinase (PFK), PKM1, or the liver isoform of pyruvate kinase (PKL) in glomeruli (Supplementary Fig. 6a–c). Consistently, we found that BCAA addition significantly upregulated the mRNA expression of *Pkm2* but not *Pkm1* in primary podocytes (Supplementary Fig. 6d–e). We then focused on the effect of BCAAs on PKM2, as PKM2 is the last rate-limiting enzyme of glycolysis that can affect glycolysis, serine biosynthesis, and glucose OXPHOS[34]. The pyruvate kinase activity of PKM2 is dynamically regulated between a hyperglycolytic active tetramer and a less active dimer[35]. PKM2 phosphorylation at serine 37 (Ser 37) or tyrosine 105 (Tyr 105) leads to PKM2 depolymerization and inactivation[36,37]. Indeed, we found that BCAAs significantly increased the dimer and monomer levels of PKM2 in LG cultured primary podocytes (Fig. 5c) and significantly increased the phosphorylation of PKM2 at both Ser 37 and Tyr 105 (Fig. 5d). Besides, BCAAs enhanced PKM2 dimer and monomer formation in HG condition (Fig. 5e). Then, we tested pyruvate kinase activity in vitro and found that BCAA supplementation significantly inhibited pyruvate kinase activity in podocytes (Fig. 5f). Fructose metabolite F-1-P is known to inhibit PKM2 tetramer formation[38], we then detected the mRNA levels of fructose metabolic enzymes and found BCAAs significantly only increased adolase B expression (Supplementary Fig. 6f), which is responsible for F-1-P degradation. Thus, F-1-P may not be the mediator leading to PKM2 depolymerization. These results suggest that BCAAs promote PKM2 phosphorylation and lead to PKM2 depolymerization and inactivation.

To test the causal relationship between PKM2 depolymerization/inactivation and the glucose metabolic switch in BCAA-treated podocytes, we utilized the PKM2 activator TEPP46 and assessed cellular glucose metabolism with a Seahorse assay. As shown in Fig. 5g, TEPP46 administration significantly increased pyruvate kinase activity in the HG/BCAA-treated podocytes. ECAR analysis revealed that TEPP46 administration significantly increased the post-oligomycin A and the reserved capacity of ECAR but did not increase the post-glucose of

https://doi.org/10.1038/s41467-025-62890-9

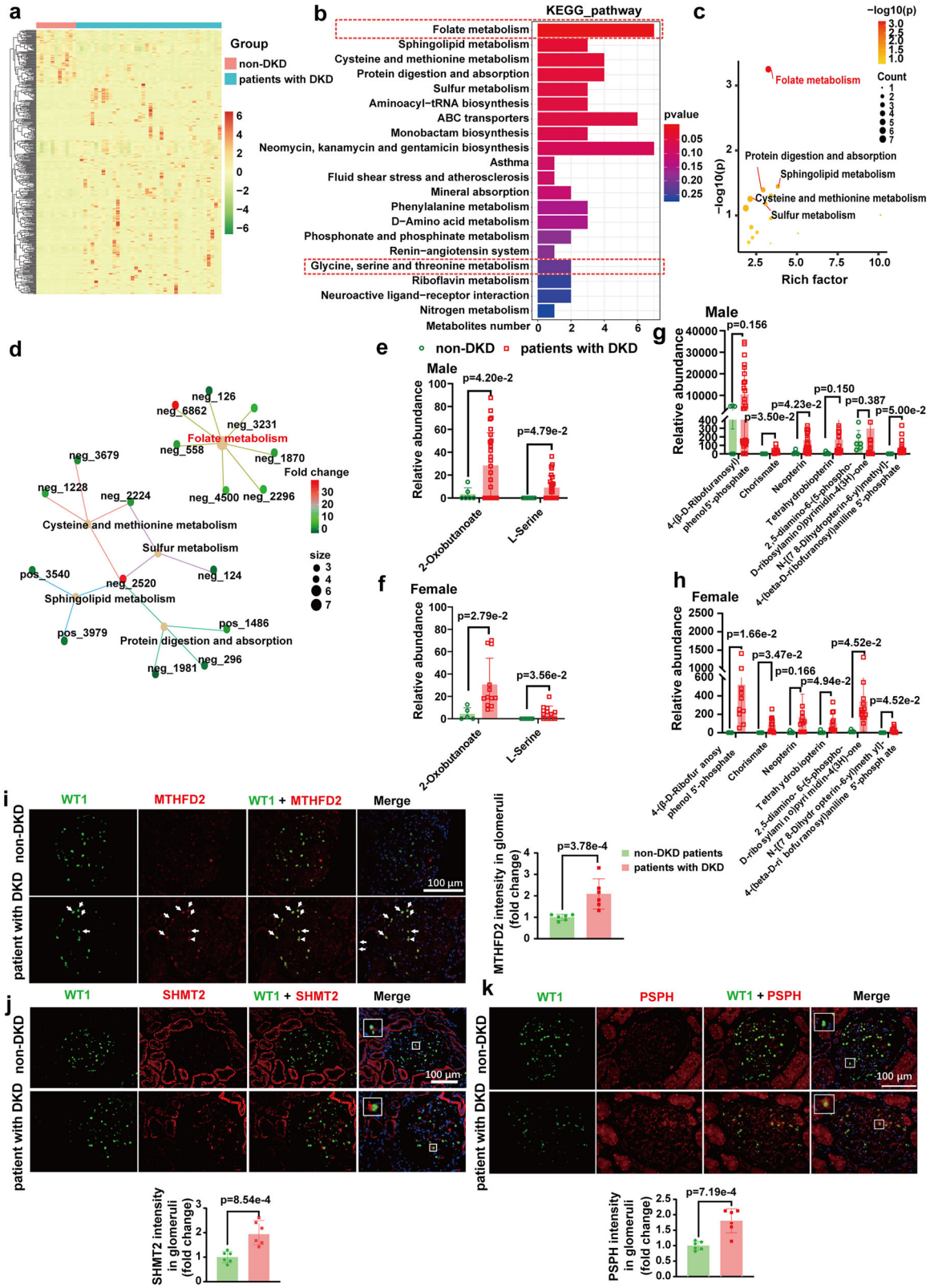

ECAR in the HG/BCAA-treated podocytes (Fig. 5h). OCR analysis revealed that TEPP46 addition significantly reversed the decreases in basal respiration, ATP-coupled respiration, maximal respiration, and reserve respiration capacity induced by HG/BCAAs (Fig. 5i). These results showed that administration of the PKM2 activator TEPP46 significantly restored BCAA-mediated suppression of glucose OXPHOS in podocytes.

To confirm the role of PKM2 in BCAA-induced glucose metabolic disorders in podocytes, we conducted RNA sequencing analysis. Gene Ontology analysis indicated that TEPP46 treatment increased the cellular component movement, cell motility, cell migration, epithelial cell differentiation and actin cytoskeleton pathways (Fig. 5j). Indeed, we found that TEPP46 administration reversed BCAA-induced down-regulation of the expression of skeletal genes (*Tubb2b, Tuba4a*, and

Fig. 4 | Serine biosynthesis and folate metabolism were significantly increased in DKD kidneys. We collected urine samples from T2DM patients without or with DKD, and analyzed the urinary metabolites by nontargeted metabolomics. **a** Heatmap of nontargeted urinary metabolomics showing the differentially abundant metabolites between non-DKD patients ($n = 11$) and patients with DKD ($n = 40$). **b** Enriched bar plots of KEGG pathways showing 20 pathways that differed between the non-DKD ($n = 11$) and DKD ($n = 40$) groups. The red dashed boxes indicate the folate metabolism pathway and glycine, serine, and threonine metabolism pathways. **c** Enrichment factor analysis showed that folate metabolism was the most-enriched pathway between the non-DKD and DKD groups according to the p value. **d** Enriched cnet plots of KEGG pathways showing that the abundances of 7 metabolites from the folate metabolism pathway were significantly different between the non-DKD ($n = 11$) and DKD ($n = 40$) groups. **e, f** Two metabolites of serine biosynthesis (2-oxobutanoate and L-serine) showed significantly upregulated in the DKD group, Male: $n = 6$ for non DKD, $n = 28$ for DKD group; Female: $n = 5$ for non DKD, $n = 12$ for DKD group. **g, h** Six intermediate metabolites from folate metabolism were measured in the DKD group, Male: $n = 6$ for non DKD, $n = 28$ for DKD group; Female: $n = 5$ for non DKD, $n = 12$ for DKD group. **i–k** Representative images of double staining of MTHFD2, SHMT2 or PSPH with that of WT-1 and measurement of MTHFD2, SHMT2, and PSPH expression in glomerular sections. A total of 70 glomeruli from $n = 6$ mice per group. Arrow and white box indicate the localization of WT1 with MTHFD2, SHMT2, or PSPH. The data were presented as mean ± SD, and analyzed by unpaired two-tailed Student's t test.

Tuba1a) and metalloproteinase genes (*Met*, *Sema3c* and *Adamts1)* in vivo (Fig. 5k). TEPP46 administration also restored the decreased organization of F-actin filaments in podocytes treated with HG/BCAA (Fig. 5l). In addition, TEPP46 administration reversed the BCAA-induced upregulation of metabolic pathways (Fig. 5j). Further analysis of the differentially expressed genes in podocytes with a cutoff of a fold change ≥ 1.5 (HG/BCAA versus HG/BCAA + TEPP46) and $P < 0.05$ revealed that TEPP46 treatment reversed the changes in the expression of 27 out of 33 genes which expression was upregulated by BCAA supplementation (Fig. 5m). Importantly, the expression of these genes was strongly correlated with serine biosynthesis and folate metabolism (Fig. 5n). Indeed, TEPP46 administration partially eliminated BCAA-induced serine and folate synthesis, as demonstrated by the down-regulation of the mRNA and/or protein expression levels of Phgdh, Shmt2, Psph, Mthfd2, Slc1a4, and Slc1a5 (Fig. 5n–p). Overall, we demonstrated that BCAA administration inhibited PKM2 pyruvate kinase activity, which blocks glucose OXPHOS and promotes a shift in glucose metabolism to serine biosynthesis and folate metabolism.

BCAA administration induced podocyte apoptosis by promoting PKM2-DDIT3 cotransport into the nucleus to activate the transcription of Chac1 and Trib3

In addition to pyruvate kinase activity in the cytoplasm, nuclear-localized PKM2 can regulate transcriptional activity as a cotranscription factor[39]. In addition, the phosphorylation of PKM2 at Ser 37 was reported to promote PKM2 translocation to the nucleus[37]. As shown in Fig. 5d, BCAA administration significantly increased the phosphorylation of PKM2 at Ser 37. We then observed the subcellular localization of PKM2 in podocytes by performing immunostaining and immunoblotting. We found that HG/BCAA significantly increased PKM2 expression in the nucleus of podocytes, as compared to HG group (Fig. 6a, b), suggesting that BCAA supplementation promoted PKM2 nuclear translocation in podocytes. We reanalyzed the RNA-seq data and found that BCAA-upregulated genes are reported to be primarily controlled by the transcription factors ATF5, ATF4, and DDIT3 (Fig. 3d, e)[40,41]. We conducted coimmunoprecipitation (IP) with a PKM2 antibody and found that PKM2 did not bind to ATF4 or ATF5 (Fig. 6c) but bound to DDIT3 in both whole-cell and nuclear extracts (Fig. 6c, d). High sensitivity structured illumination microscope (HiS-SIM) also showed co-localization of PKM2 and DDIT3, which was enhanced by BCAAs addition (Supplementary Fig. 7a). Bioinformatics prediction with HDOCK showed that PKM2 and DDIT3 may form two protein interaction interfaces with Ser (S) 14, Glu (E) 17, Asn (N) 44, Arg (R) 156, and His (H) 166 as the interaction hotspots from DDIT3, H81, Asp (D) 101, E131, S202 and Lys (K) 504 as the interaction hotspots from PKM2 (Supplementary Fig. 7b). We then constructed a wild type (WT) DDIT3 plasmid and a mutant DDIT3 plasmid in S14, E17, N44, R156 and H166 amino acids residues that fused to 3 x Flag (Supplementary Fig. 7c). IP assay confirmed that mutant DDIT3 did not bind with PKM2 (Supplementary Fig. 7d). Besides, we constructed adenoviruses harboring wild type (WT) PKM2 or mutant PKM2 in H81, D101, E131, S202, and K504 amino acids residues that fused to HA tag, IP assay confirmed that mutant PKM2 did not bind with DDIT3, either affected the protein level of DDIT3 (Supplementary Fig. 7e and f). In addition, Chac1 and Trib3, two DDIT3-targeting genes, were among the top upregulated genes in BCAA-treated podocytes (Fig. 3d). Therefore, we hypothesized that, as a cotranscriptional factor, PKM2 binds to DDIT3 in the nucleus and regulates its transcriptional activity. We subsequently conducted a chromatin immunoprecipitation (ChIP) assay. The ChIP results indicated that PKM2 bound to the Trib3 promoter, which was significantly blocked by DDIT3 knockdown (Fig. 6e), suggesting that DDIT3 is required for the binding of PKM2 to the Trib3 promoter. In addition, PKM2 overexpression increased DDIT3 binding to Trib3 promoter (Fig. 6f). We further determined Chac1 and Trib3 expression in PKM2-overexpressing or PKM2-knockout podocytes. Indeed, PKM2 overexpression upregulated Chac1 and Trib3 protein expression, while PKM2 knockout decreased their protein expression (Fig. 6g). As shown in Fig. 6h, PKM2 knockout significantly inhibited BCAA-induced upregulation of Chac1 and Trib3 expression. These results demonstrate that PKM2 regulates the transcriptional activation of DDIT3 upon Chac1 and Trib3.

Since we showed that PKM2 binds to DDIT3 in the nucleus (Fig. 6d), we then investigated whether PKM2 and DDIT3 are cotransported into the nucleus in podocytes after HG/BCAA challenge. TEPP46, a PKM2 agonist, was utilized to restore the PKM2 tetramer and block PKM2 translocation into the nucleus[42]. Indeed, TEPP46 administration significantly reduced nuclear PKM2 and DDIT3 protein levels in HG/BCAA-treated podocytes, as evidenced by both immunoblotting and immunostaining (Fig. 6i, j). Meanwhile, TEPP46 significantly increased PKM2 and DDIT3 protein levels in the podocyte cytoplasm compared to those in the HG/BCAA group (Fig. 6i). Consistently, HiS-SIM showed that TEPP46 enhanced cytoplasmic co-localization of PKM2 with DDIT3, and inhibited their co-localization in nucleus (Supplementary Fig. 7a). Furthermore, TEPP46 administration significantly restored podocyte viability (Fig. 6k) and significantly decreased Chac1 and Trib3 protein levels in HG/BCAA-treated podocytes (Fig. 6l). Collectively, these data demonstrate that BCAA administration promotes PKM2/DDIT3 binding and nuclear cotransport and regulates DDIT3-mediated transcriptional activation of Chac1 and Trib3, which contributes to BCAA catabolic defect-induced podocyte apoptosis.

Treatment with the PKM2 agonist TEPP46 or activation of BCAA catabolism attenuates renal injury in DKD mice

To confirm that PKM2 depolymerization and inactivation mediate podocyte injury and DKD progression, the PKM2 agonist TEPP46 was used as a therapeutic strategy. We found that TEPP46 administration significantly increased pyruvate kinase activity in the HF/BCAA diet-fed mice (Fig. 7a). TEPP46 treatment significantly increased the mRNA expression levels of glomerular *Synpo, Nephrin*, *P-cadherin,* and *Nphs2* (Fig. 7b) and the protein expression levels of Synpo and Nphs2 in the HF/BCAA-fed mice (Fig. 7c, d). TEPP46 administration also significantly increased the number of podocytes (Fig. 7e), decreased podocyte apoptosis (Fig. 7f), and decreased the protein expression of Chac1 and Trib3 in glomeruli isolated from the HF/BCAA-fed mice (Fig. 7c). TEM revealed that TEPP46 administration significantly decreased BCAA

https://doi.org/10.1038/s41467-025-62890-9

supplementation-induced GBM thickening and foot process fusion (Fig. 7g). These data suggested that administration of the PKM2 agonist TEPP46 significantly alleviated BCAA supplementation-induced podocyte dysfunction and death.

In addition, TEPP46 administration substantially inhibited BCAA supplementation-induced tubular cast formation and mesangial matrix expansion in the HF/BCAA diet-fed obese mice, as indicated by PAS staining (Fig. 7h, i). TEPP46 administration reversed BCAA supplementation-induced renal lipid droplets accumulation, as demonstrated by renal oil red O staining, triglyceride quantification and TEM analysis (Fig. 7j, k). Moreover, TEPP46 significantly decreased the kidney weight-to-body weight ratio and improved the urinary albumin/creatinine ratio in the HF/BCAA diet-fed mice (Fig. 7l, m). Next, we constructed podocyte-specific PKM2 KO (PKM2$^{f/f}$ Cre^{+}) mice

Fig. 5 | BCAAs elicited podocyte metabolic reprogramming by inducing PKM2 depolymerization and inactivation. a, b The protein expression of GCK, PFK, PKM1, and PKM2 in primary podocytes (**a**) and isolated glomeruli (**b**) from mice. **c** Representative Western blots of cross-linked PKM2 in primary podocytes, $n = 3$. Tetra, tetramer; Di, dimer; Mono, monomer. **d** Representative Western blots of PKM2 phosphorylation in primary podocytes. **e** Representative Western blots of cross-linked PKM2 in primary podocytes, 20 mM mannitol (Man) plus 5 mM glucose were used as osmotic control, $n = 3$. **f, g** Relative pyruvate kinase activities in primary podocytes. $n = 6$. **h** Upper, ECAR in primary podocytes were determined; bottom: measurements of the post-glucose, post-oligomycin A, and reserved capacity of ECAR. $n = 5$. **i** Upper, OCR of primary podocytes were determined; bottom, statistical analyses of baseline respiratory capacity, ATP-coupled respiratory capacity, maximum respiratory capacity, and reserve respiratory capacity in the OCR. 2-DG, 2-deoxyglucose. FCCP, cyanide-4-(trifluoromethoxy) phenylhydrazone. RE, rotenone. Resp, respiration. $n = 5$. **j** Enrichment pathway analysis via RNA sequencing of MPC-5 podocytes (HG/BCAA + TEPP46 vs HG/BCAA) revealed the top 7 pathways with upregulated component expression (red) and the top 7 pathways with downregulated component expression (green) using Gene Ontology (GO) annotations and modified Fisher's exact test. The numbers in parentheses indicate the number of genes in each GO term biological process. **k** The mRNA expression of skeleton-related genes in primary podocytes. $n = 6$ mice. **l** Representative immunofluorescence images of F-actin expression in differentiated MPC-5 podocytes. **m** The expression of 27 out of 33 genes whose expression in the HG/BCAA group was reversed by administration of 10 μM TEPP46. The numbers on the right of the heatmap indicate the fold changes. The data were analyzed by the Mann–Whitney U test. **n** Schematic metabolic map of glucose metabolism in podocytes treated with HG, HG/BCAA, or HG/BCAA + TEPP46. **o** The mRNA expression of the indicated genes in primary podocytes. $n = 6$. **p** Protein expression in isolated glomeruli from mice. The data were presented as mean ± SD, and analyzed by unpaired two-tailed Student's t test (**j, m**) or one-way ANOVA (**f–i, k, o**).

by breeding PKM2 floxed mice with Nphs2 Cre mice (Supplementary Fig. 8a–c). Podocyte-specific PKM2 KO did not affect fasting glucose levels or glucose/insulin tolerance (Supplementary Fig. 8d–f). Importantly, podocyte-specific PKM2 KO completely blocked the renoprotective effect of TEPP46 on the HF/BCAA diet-fed mice (Fig. 7n–q). Collectively, these results demonstrate that the PKM2 agonist TEPP46 increases the survival and function of glomerular podocytes and alleviated HF/BCAA diet-induced renal injury by activating PKM2 in podocytes.

To confirm whether activating BCAA catabolism reduces renal injury in DKD, we used the BDK inhibitor compound 3,6-dichlorobenzo[b]thiophene-2-carboxylic acid (BT2)[43] to promote BCAA catabolism from 6 to 22 weeks in db/db mice. BT2 administration significantly decreased plasma BCAA levels in db/db mice (Supplementary Fig. 9a) and improved the kidney weight-to-body weight ratio (Supplementary Fig. 9b). BT2 administration substantially alleviated renal tubule cast formation, mesangial expansion, and renal lipid droplets accumulation as indicated by TG measurements and Oil red O staining in db/db mice (Supplementary Fig. 9c–e). In addition, BT2 administration markedly reduced urinary albumin excretion for 24 h and improved plasma creatinine, uric acid, and urea nitrogen levels in db/db mice (Supplementary Fig. 9f–i). Furthermore, activating BCAA catabolism by BT2 administration partially prevented podocyte loss, as indicated by TUNEL staining and podocyte number calculations (Supplementary Fig. 9j, k), and alleviated podocyte injury, as indicated by the upregulated expression of Nphs2 and Synpo (Supplementary Fig. 9l, m). These data confirmed that activating BCAA catabolism prevents the development of DKD in db/db mice.

Discussion

DKD occurs in approximately 30-40% of patients with diabetes. Hyperglycemia and hypertension have long been recognized as the main causes of DKD progression. However, intensive glycemic control and strict blood pressure control have limited beneficial effects on the initiation of DKD and the progression of DKD to ESRD[44,45]. Therefore, identifying the potential missing factors that determine the initiation of DKD is valuable for DKD prevention and therapy.

BCAAs are a group of essential amino acids that are physiologically utilized to build blocks for protein synthesis and control energy homeostasis[46,47]. Data from our laboratory and other laboratories have demonstrated that BCAA catabolic defects not only contribute to the development of insulin resistance and diabetes[13,15,48], but also lead to heart and liver injury[16,49]. However, whether BCAA catabolic defects contribute to DKD progression remains unclear. Serum BCAA levels decrease with the progression of albuminuria[50]. Moreover, plasma BCAA levels are decreased in advanced chronic kidney disease (CKD) patients due to hypermetabolism and metabolic acidosis, which affect the whole-body nitrogen balance[51–53]. For a long time, essential amino acids or ketoacid analogs (including BCAAs or branched-chain α-keto acids) have been recommended as nutritional supplements for advanced CKD patients who are prescribed a very low-protein diet[54]. These findings may lead to the ignorance of the role of BCAAs in DKD development. Recently, high plasma and urinary BCAA metabolites were shown to predict the future risk of DKD[17,55]. Determining the role of BCAAs in DKD initiation/progression and the underlying mechanisms is highly important.

In the present study, we made several novel observations. First, we found that glomerular podocytes exhibit BCAA catabolic defects in patients with DKD and DKD animal models (Fig. 8). As reported, the activity of renal BCKD, the rate-limiting catabolic enzyme of BCAAs, is in a level second only to that of the liver throughout the body[56]. To elucidate the role of BCAA catabolism in the glomeruli, we tested the location and activity of the rate-determining enzyme BCKD, as well as its regulatory enzymes PP2Cm and BDK. We showed that podocytes express relatively high levels of BCKD, PP2Cm, and BDK. Mature podocytes are rich in mitochondria[57], where most BCAA-catabolic enzymes primarily exist[58]. This finding may be the reason that podocytes have a high BCAA oxidative capacity. Here, we showed that in podocytes from patients with DKD and DKD model mice, BCKD activity is significantly decreased, as indicated by increased P-BCKDE1α (Ser 293) expression. Interestingly, the levels of the upstream regulatory molecules PP2Cm are decreased in podocytes from patients with DKD and DKD mice. HG reportedly reduces the expression of KLF15 and inhibits BCAA degradation in cardiomyocytes[59]. The downregulation of PP2Cm is likely responsible for the increase in P-BCKDE1α (Ser 293) in podocytes of patients with DKD and DKD mice. Besides, the BCAAs and BCKAs levels in isolated glomeruli were significantly increased in db/db mice. These results are consistent with previous proteomic data in isolated glomeruli from DKD and non-DKD patients with >50 years of age with diabetes, which showed that BCAA oxidation pathways have tendency to be downregulated in patients with DKD[28]. BCAAs catabolic pathways are also suppressed in acute kidney injury and fibrosis[29,60,61]. We confirmed for the first time that there is a BCAA catabolic defect in glomerular podocytes under DKD conditions.

Second, we found that podocyte BCAA catabolic defects cause renal injury in mice with DKD (Fig. 8). Previously, evidence from our group and other researchers demonstrated that BCAA accumulation causes cardiomyocyte and hepatocyte injury[16,49,62]. Here, using HF diet-induced diabetic mice and BCAA overload models (mice in which podocyte-specific PP2Cm was deleted or BCAAs were exogenously supplemented to HF diet-fed mice), we demonstrated that BCAA accumulation plus a HF diet successfully induced DKD phenotypes, as characterized by proteinuria, glomerular abnormalities, lipid droplets accumulation, and renal filtration membrane injury. HF diet feeding alone did not induce renal injury in C57BL/6 mice. These data

https://doi.org/10.1038/s41467-025-62890-9

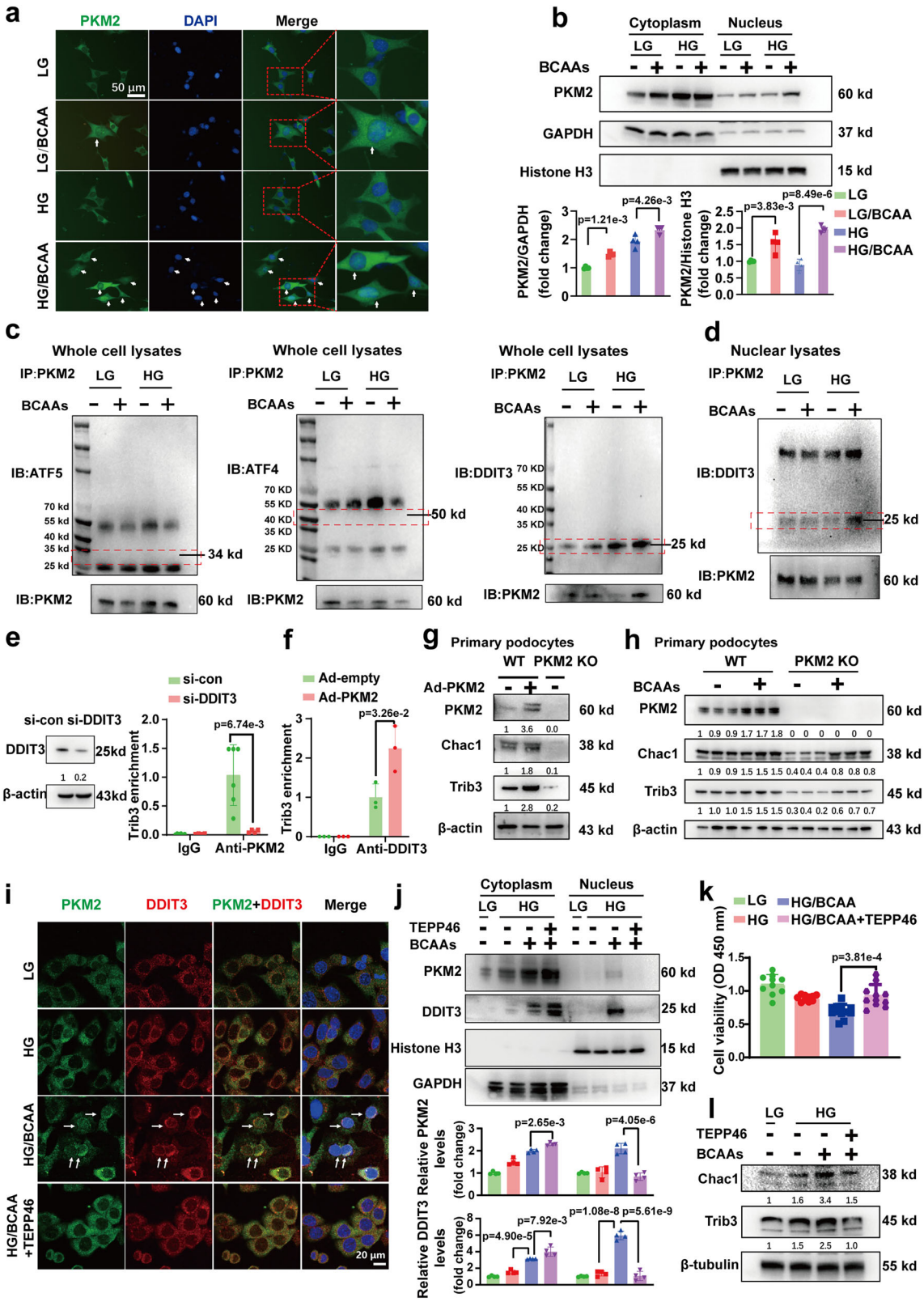

suggested the key role of BCAA catabolic defects in the development of DKD. In addition, we showed that BCAA catabolic defects cause podocyte dysfunction and apoptosis, as evidenced by increased foot process fusion, decreased expression of podocyte-specific markers, dysregulated actin cytoskeleton, and reduced podocyte number in DKD animals. Podocyte injury is considered the most important early event contributing to DKD. Podocyte dysfunction and loss are major contributors to proteinuria and DKD development[63]. Podocytes form the epithelial surface of the glomerulus and interdigitate with each other at their foot process through a specialized intercellular junction called a slit diaphragm. Nphs2 and Nephrin are the main components of the slit diaphragm. Nphs2 and Nephrin loss leads to podocyte dysfunction and proteinuria[64]. Another podocyte-specific protein, Synpo, orchestrates actin organization and podocyte motility[65]. Dysregulated

Fig. 6 | BCAAs induce podocyte apoptosis by promoting PKM2-DDIT3 cotransport into the nucleus to promote Chac1 and Trib3 transcription. a PKM2 expression (green) and nuclei (blue) were detected by fluorescence microscope in LG-, HG- or HG/BCAA-treated differentiated MPC-5 podocytes. **b** Quantification of the protein expression of PKM2 in the cytoplasm and nucleus of differentiated MPC-5 podocytes. $n = 4$ total samples per group. **c, d** Coimmunoprecipitation (IP) and immunoblotting (IB) analysis of PKM2 with ATF5, ATF4, and DDIT3 in whole-cell or nucleus lysates of differentiated MPC-5 podocytes. **e** Chromatin immunoprecipitation (ChIP) assay of PKM2 with th.e Trib3 promoter in MPC-5 podocytes treated with DDIT3 siRNA (si-DDIT3) or scramble RNA (si-con). $n = 6$. **f** ChIP assay of DDIT3 with the Trib3 promoter in MPC-5 podocytes treated with Ad-PKM2 or Ad-empty. $n = 3$. **g** Representative Western blots of PKM2, Chac1, and Trib3 expression in primary podocytes isolated from PKM2 knockout mice (KO) or wild-type mice and transfected with adenovirus overexpressing PKM2 (OE) or empty vector (-). **h** Representative Western blots of PKM2, Chac1, and Trib3 expression in primary podocytes isolated from PKM2 KO mice that were exposed to 3 mM BCAAs for 24 h. **i, j** Representative confocal immunofluorescence images (**i**) and Western blots (**j**) of differentiated MPC-5 podocytes that were exposed to LG, HG, and/or 3 mM BCAA or 20 nM TEPP46 for 24 h. Both cytoplasmic and nuclear extracts were evaluated. $n = 4$ total samples per group. **k, l** Cell viability (**k**, $n = 10$ for LG and HG; $n = 12$ for HG/BCAA, $n = 11$ for HG/BCAA + TEPP46) and protein expression of Chac1 and Trib3 (**l**, $n = 4$ total samples per group) in differentiated MPC-5 podocytes were determined. The data were presented as mean ± SD, and analyzed by unpaired two-tailed Student's t test (**e, f**) or one-way ANOVA (**b, i,** and **j**).

actin cytoskeleton directly results in foot process dysfunction and contributes to albuminuria[66]. We showed that BCAA supplementation disrupted actin filament organization in podocytes and decreased the expression of podocyte-specific genes, such as Nphs2, Nephrin, and Synpo, and genes involved in actin skeleton arrangement. Pharmacological activation of BCAA catabolism using the BDK inhibitor BT2 significantly alleviated podocyte dysfunction, increased the number of podocytes by inhibiting their apoptosis, and restored renal function in the db/db model. Therefore, we provide the first direct evidence that BCAA catabolic defects and overload contribute to DKD development by inducing podocyte injury and loss.

Third, we found that BCAA accumulation induces podocyte metabolic remodeling and dysfunction (Fig. 8). Through RNA-seq analysis, Seahorse, and ^{13}C-labeled glucose metabolic flux analyses, we found that BCAA supplementation inhibited glucose OXPHOS and promoted a shift in glucose metabolism to serine biosynthesis and folate metabolism in podocytes. Consistently, we found significantly increased levels of urinary serine and folate biosynthetic intermediate metabolites in patients with DKD. The expression of key enzymes involved in both folate metabolism and serine biosynthesis is also significantly increased in the podocytes of patients with DKD. Emerging evidence shows that BCAA metabolic disorders disrupt cellular energetic metabolism[26]. We previously demonstrated that BCAA catabolic defects affect glucose and lipid metabolism[15,16,49]. BCAA catabolic defects directly inhibit glucose oxidation by suppressing pyruvate dehydrogenase complex activity[62]. Our results are consistent with previous studies showing that BCAAs inhibit glucose OXPHOS. Podocytes are terminally postmitotic cells that are highly dependent on glucose catabolism for substantial fuel supply. A considerable number of mitochondria have been observed in the cell body and narrow peripheral foot processes of podocytes[67]. Mature podocytes preferentially rely on OXPHOS for their energy demands[68]. OXPHOS suppression leads to decreased Nephrin expression in podocytes[69]. Moreover, glycolysis is required for the formation of lamellipodia, local ATP formation in cell processes, and cell migration[70]. In the present study, we demonstrated that under diabetic conditions, BCAAs inhibit glucose catabolism and mediate a shift to amino acid and folate anabolism in podocytes, which may cause podocyte energy deficit and dysfunction.

As a low molecular weight compound, folic acid or folate is freely filtered by the glomerulus. While a low dose of folic acid is nutritionally beneficial, a high dose of folic acid is very toxic to the kidneys[71]. Folic acids induce renal injury through oxidative stress, impaired mitophagy and mitochondrial bioenergetics, ferroptosis, apoptosis, and pyroptosis. Previous data suggested that folic acid induces renal injury mainly in proximal tubular epithelial cells[72]. Our data suggested that podocytes, which highly express folate metabolic enzymes such as Shmt2 and Mthfd2, are also vulnerable to folic acid accumulation-induced injury. Interestingly, plasma serine levels are reduced in patients with diabetes, and low systemic serine levels are emerging as a hallmark of diabetes-related peripheral neuropathy complications[73]. Therefore, the disordered serine biosynthesis and folate metabolism in podocytes induced by BCAA catabolic defects may also be an indicator and a contributor to DKD initiation or progression.

Fourth, we found that PKM2 depolymerization and inactivation mediated BCAA-induced podocyte metabolic remodeling and dysfunction (Fig. 8). By screening key glycolytic enzymes, we found that PKM2 is sensitive to BCAA levels. BCAAs upregulated PKM2 expression but promoted PKM2 phosphorylation, depolymerization, and inactivation, which inhibited glucose OXPHOS and promoted a shift in glucose metabolism to serine biosynthesis and folate metabolism. PKM2 expression can be dynamically shifted between the less active PKM2 dimer and the highly active PKM2 tetramer[35]. PKM2 may act as an amino acid sensor, and some amino acids may allosterically regulate PKM2 activity[74]. Interestingly, valine acts as an inhibitor[74], while serine is a natural ligand and allosteric activator of PKM2[75]. Here, we show that PKM2 exists as a central point of metabolic regulation involved in glucose oxidation, glycolysis, and serine or folate metabolism. PKM2 depolymerization subsequently activates the serine and folate biosynthetic pathway. However, the underlying mechanisms by which BCAAs lead to PKM2 depolymerization and inactivation need to be further studied.

Finally, we demonstrated that BCAAs promote PKM2-DDIT3 cotransport to the nucleus and transcriptionally upregulate the expression of the DDIT3 target genes Chac1 and Trib3, which induce podocyte apoptosis (Fig. 8). Through RNA-seq data analysis and co-immunoprecipitation screening, we found that BCAA administration increased the binding of PKM2 to DDIT3 and increased the transcriptional activity of DDIT3. Via a ChIP assay, we confirmed that PKM2 binds to DDIT3 on the Trib3 promoter region. Chac1 and Trib3 are downstream effectors of DDIT3 that mediate DDIT3-dependent cell death[76,77]. Overall, BCAA administration promoted PKM2 depolymerization and inactivation. Depolymerized PKM2 loses its pyruvate kinase activity and suppresses glucose OXPHOS; conversely, depolymerized PKM2 is cotransported to the nucleus with DDIT3, where it acts as a novel cotranscriptional factor and promotes DDIT3 transcriptional activity. DDIT3 transcriptionally promotes Chac1 and Trib3 expression, which directly elicits podocyte apoptosis. Activating PKM2 by TEPP46 administration has dual beneficial effects on podocyte apoptosis and metabolic dysfunction.

To mimic the initiation or development of DKD from T2DM in mice, 60% high-fat diets were utilized to induce obese/T2DM model in vivo. However, in cell culture experiments, we focused on the glucose metabolism of podocytes due to their distinct anatomical position and unique energetic metabolic characteristics. Podocytes are located at the outermost layer of the glomerular filtration barrier, where they are directly exposed to the glomerular ultrafiltrate in the primary urine. The glucose concentration in the primary urine is comparable to that in the blood, as the glomerular filtration barrier is freely permeable to glucose. However, fatty acids cannot pass the glomerular filtration membrane barrier because they are bound to albumin and transported in the bloodstream. Moreover, podocytes

https://doi.org/10.1038/s41467-025-62890-9

predominantly depend on glucose-driven oxidative phosphorylation for energy supply[68]. Dysregulation of glucose metabolism is a key contributor to the development of DKD[28].

The BDK inhibitor BT2 and PKM2 agonist TEPP46 were utilized. As a specific and robust BDK inhibitor, BT2 has excellent pharmacokinetics (terminal T1⁄2 730 min) and metabolic stability (no degradation in 240 min)[43] with IC50 (3.19 μM) and high plasma protein bound percentage (99.3%). Recently, BT2 is reported to act as a mitochondrial uncoupler[78], which may attenuate ROS production. But the effect is mild considering the limited free plasma BT2 concentrations and mild uncoupling effect (roughly six-fold less potent than 2,4-dinitrophenol (DNP). TEPP46 is a well-documented selective activator of PKM2[28,42]. Pharmacokinetic parameters of TEPP-46 in male Balb/c mice following intravenous administration exhibit relatively low clearance and long half-life (T1/2 5.8 hrs, CL 17.1 ml/min/kg)[79]. The off target of TEPP46 is known to partially activate PKM1 or PKL[79]. In the present study,

Fig. 7 | TEPP46 administration reversed BCAA supplementation-induced renal injury in HF diet-induced obese mice. a Pyruvate kinase activity in glomeruli isolated from mice. $n = 8$ mice per group. **b** The mRNA expression of *Synpo*, *Nephrin*, *P-cadherin*, and *Nphs2*. $n = 5$ mice for Nphs2 in HF/Paired group, $n = 6$ mice for others. **c** Representative immunoblotting of Nphs2, Synpo, Chac1 and Trib3 ($n = 4$ for HF/Paired group, $n = 5$ for HF/BCAA and HF/BCAA + TEPP46 groups). **d** Left: Representative immunofluorescence images of Nphs2 (green) and Synpo (red). Right: quantification of Nphs2 and Synpo intensities per glomerulus. In each group, 70 glomeruli from 6 mice were evaluated. **e** Representative immunostaining images of WT1-positive podocytes and quantification of WT1-positive podocytes in renal sections from mice. In each group, 60-89 glomeruli from 6 mice were evaluated. **f** Representative images of TUNEL staining and quantification of glomerular apoptotic cells in mouse renal sections. A total of 55-97 glomeruli from 6 mice per group were evaluated. **g** Representative transmission electron microscopy (TEM) images and quantification of the thickness of the glomerular basement membrane (GBM) and foot process width. An average of 120 measurements were performed for each mouse, $n = 8$ mice per group. **h** Representative PAS staining of kidney sections (the arrows indicate tubule casts). **i** Representative PAS staining of the glomeruli of mice and quantification of mesangial matrix expansion was showed. An average of 60 glomeruli per group was assessed. $n = 8$ per group. **j** Oil red O staining of kidney sections and TEM analysis of primary proximal tubular cells from kidney sections. Red triangles indicate lipid droplets. **k** Renal TG levels in kidney tissue. $n = 8$. **l** The kidney weight to body weight ratio. $n = 8$. **m** The urinary albumin/creatinine ratio. $n = 11$ mice per group. **n–q** Wild type C57BL/6 mice, $PKM2^{f/f}$, and $PKM2^{f/f}$ Cre^{+} mice were fed the indicated food for 16 weeks, and TEPP46 were treated daily by oral gavage at 30 mg/kg body weight in indicated group. Plasma uric acid, plasma creatinine, urea nitrogen, and urinary albumin levels were measured. $n = 8$ per group. The data were presented as mean ± SD, and analyzed by one-way ANOVA.

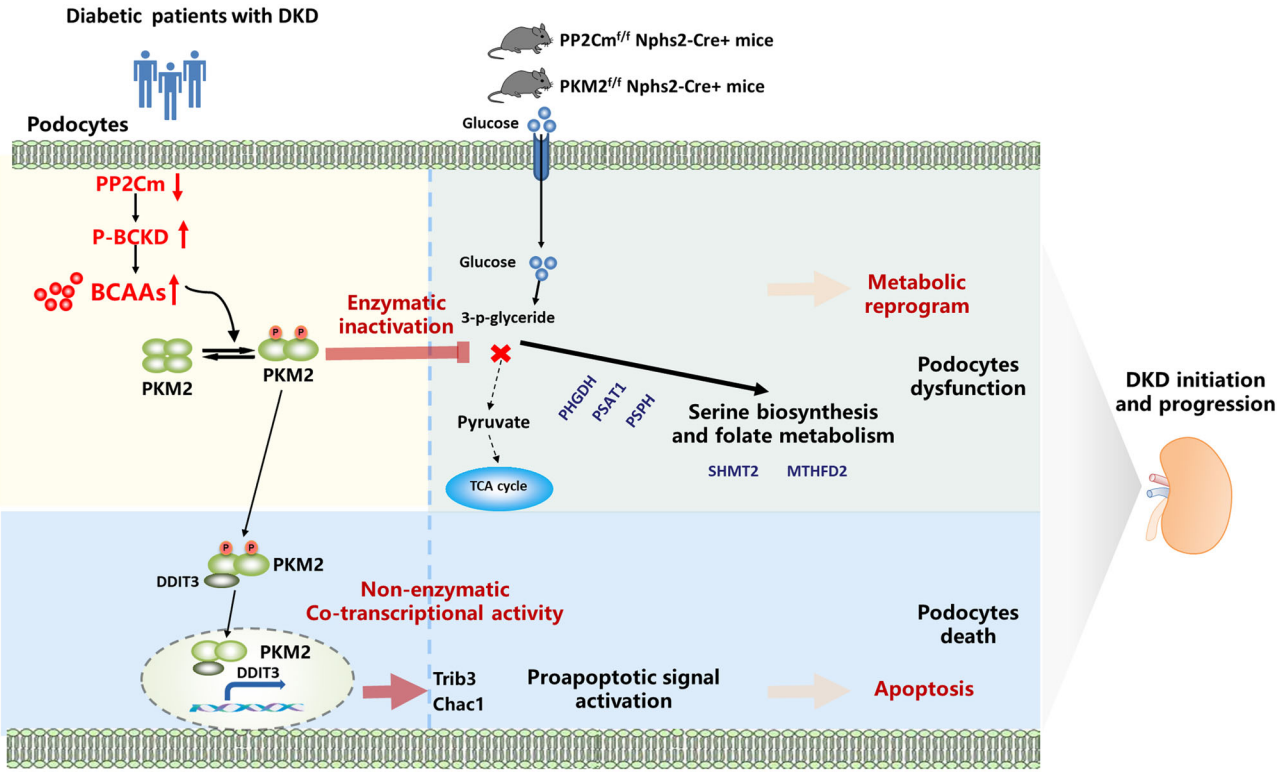

Fig. 8 | The role of podocytes BCAAs catabolic defects upon DKD progression. Glomerular podocytes in male and female patients with DKD and db/db mice specifically display BCAA catabolic defects. BCAA catabolic defects contribute to DKD development by inducing renal podocyte metabolic remodeling and apoptosis. BCAA catabolic defects result in podocyte PKM2 depolymerization and inactivation, which inhibits glucose OXPHOS and promotes a shift in glucose metabolism to serine biosynthesis and folate metabolism. BCAA promotes PKM2-DDIT3 binding, nuclear co-transportation, and regulates DDIT3 transcriptional activation of Chac1 and Trib3, which induce podocyte apoptosis.

podocyte-specific PKM2 KO completely blocked the renoprotective effect of TEPP46 on the HF/BCAA diet-fed mice (Fig. 7n–q), which suggested that TEPP46 produce renal protective effects through activating podocyte PKM2.

In summary, our data provide direct evidence showing that glomerular podocytes specifically exhibit BCAA catabolic defects, which play crucial roles in the initiation and progression of DKD. Mechanistically, BCAA catabolic defects induce podocyte metabolic reprogramming and apoptosis by inactivating PKM2 and promoting PKM2 transcriptional activation of Chac1 and Trib3 via DDIT3, in which PKM2 exerts a novel noncatalytic function. BCAA catabolic defects in podocytes may be one of the endogenous missing factors that contribute to DKD initiation and progression. Targeting BCAA catabolism or PKM2 activation may be novel therapeutic strategies for preventing DKD progression.

Methods

The research complies with all relevant ethical regulations. Collection and use of human clinical samples, along with participant recruitment, were approved by the ethics committee of Xijing Hospital of Fourth Military Medical University. All the samples were obtained based on informed consent. And all animal experiments were approved by the Fourth Military Medical University Animal Care and Use Committee.

Human renal biopsy samples

Human renal biopsy samples were obtained from the Nephrology Department, Xijing Hospital, Xi'an, China. The protocol was approved by the Institutional Review Board of the Ethics Committee of Xijing Hospital. Written informed consent was obtained from each patient. For the DKD group, we analyzed 6 patients with clinically diagnosed T2DM with DKD. For the non-DKD group, we analyzed 6 patients with

T2DM without DKD. The sex, age, and information of those patients are listed in Table S2.

Untargeted metabolomics of human urine samples

Twenty-four-hour urine samples were collected from T2DM patients without DKD (non-DKD, $n = 11$) or from T2DM patients with DKD (DKD, $n = 40$). Urinary metabolites were measured by untargeted metabolomic profiling at Biomarker Biotechnology, China. A high-resolution mass spectrometer (Waters Xevo G2-XS QTOF) was used to collect primary and secondary mass spectrometry data. The column is Waters Acquity UPLC HSS T3 1.8 μm 2.1*100 mm. The mobile phase was composed of 0.1% formic acid–water (v/v; A) and 0.1% formic acid acetonitrile (v/v; B) in positive ion modes, 0.1% formic acid aqueous solution; Mobile phase B, 0.1% formic acid acetonitrile. The flow rate was set at 0.4 ml/min with the following optimal gradient elution condition: 0 to 7 min, 5 to 80% B; 7 to 10 min, 80 to 100%; 10 to 13 min, 100 to 100%; 0 to 3 min, 5 to 30% B; 3 to 9 min, 30 to 90%; 9 to 12 min, 90 to 100%. Dual channel data acquisition was performed with a low collision energy of 2 V and a high collision energy range of 10 ~ 40 V at a mass spectrum scanning frequency of 0.2 s. ESI ion source analysis was performed in a 2500 V (positive ion) or − 2000 V (negative ion) mode, 30 V cone voltage, 100 °C ion source temperature, 500 °C desolvent gas temperature, 50 L/h backflush gas flow rate, and a desolventizing gas flow rate of 800 L/h, Mass-to-charge ratio (m/z) acquisition range: 50–1200. Progenesis QI software was used for peak extraction, peak alignment, and other data processing operations. Theoretical fragment identification and mass deviation were within 100 ppm. The repeatability of the experimental and quality control samples was determined using principal component analysis (PCA) and Spearman correlation analysis. Classification and pathway information about the identified metabolites were obtained from the Kyoto Encyclopedia of Genes and Genomes (KEGG), Human Metabolome Database (HMDB), and Biomarker's in-house library. And identification criteria includes: Score threshold: 40 (for confidence filtering); Theoretical fragment matching: Precursor ion mass deviation: ≤100 ppm; Fragment ion mass deviation: ≤50 ppm. The high-resolution mass spectrometry (HRMS) platform provides accurate molecular mass measurements of compounds. Identification is achieved by database matching (METLIN/HMDB/Biomarker in-house libraries), MS/MS fragmentation patterns to confirm structural features, and isotopic abundance profiles for additional validation. This relative quantification is based on the response intensity of precursor ions (MS1) detected by the mass spectrometer.

Animal studies

Adult 8-week-old male and female wild-type (WT) C57BL/6 mice were purchased from the Fourth Military Medical University Animal Center. PP2Cm floxed mice ($PP2Cm^{f/f}$, stock #S-CKO-08516), PKM2 floxed mice ($PKM2^{f/f}$, stock #S-CKO-04295) and Nphs2-Cre mice (stock #C001027) were purchased from Cyagen Biosciences, Inc. (Guangzhou, China), and were then bred at the Fourth Military Medical University Animal Center. PKM2-floxed mice harbor a floxed PKM2-specific exon 10. We crossbred these two conditional knockout mouse strains with the Nphs2-Cre mouse line to obtain podocyte-specific PKM2 knockout ($PP2Cm^{f/f}$ Cre^{+}) or podocyte-specific PP2Cm knockout ($PKM2^{f/f}$ Cre^{+}) mice. $Pkm2^{f/f}$ or $PP2Cm^{f/f}$ mice were used as littermate controls.

All animal experiments were performed according to the National Institutes of Health Guidelines on Laboratory Animals and were approved by the Fourth Military Medical University Animal Care and Use Committee. All mice were raised in a temperature-controlled facility and maintained at 26 ± 2 °C and 55 ± 15% relative humidity with a constant 12-h light/dark cycle. All mice were fed for 16 weeks with free access to water or food.

For HF diet-induced obese model, only male mice were utilized, because female C57BL/6 mice are much less prone to the development of obesity and glucose intolerance caused by HF diet[80–82].

Wild-type C57BL/6 mice were randomly divided into three groups: an HF diet-fed group, an HF plus BCAA-fed (HF/BCAA, 60% high-fat diet with drinking water containing 4% BCAAs) group, and an HF/paired group in which caloric intake was matched to that of the HF/BCAA group. All mice had free access to water and were fed a high-fat diet (Rodent diet with 60 kcal% fat, D12492, Research Diets) for 16 weeks. TEPP46 (30 mg/kg body weight) was given to the mice via daily oral gavage. Body weight and food intake were monitored every 3 or 4 days and calculated as kcal/g/week. Blood was collected via the carotid artery. The tissues were collected after the animals were sacrificed and frozen immediately in liquid nitrogen.

Starting at 6 weeks of age, db/db mice on a C57BLKS/J background were randomized into two groups and received either vehicle or BT2 treatment. Wild-type C57BL/6 mice fed a normal diet (a rodent diet with 10 kcal% fat, D12450) were used as the control group. Animals were treated daily by oral gavage with BT2 (40 mg/kg/day) or an equal volume (<200 μL per day) of vehicle from 6 weeks to 22 weeks. BT2 was dissolved in DMSO and diluted in 5% DMSO, 10% cremophor EL, and 85% 0.1 mol/L sodium bicarbonate (pH 9.0) for delivery.

High-fat (HF) diet, HF/Paired, and HF/BCAA feeding

The paired-feeding protocols were performed as previously described[15,83]. To conduct a paired-feeding assay, we first assessed the total body weight of the HF/BCAA group (A [g]) and calculated the total calories consumed (B) each day (B = [total calories provided - calories in uneaten food]/day). We then determined the calories consumed per gram body weight (C [cal/g]) = (B [cal]/total body weight (A [g]). Next, we measured the total body weight (D [g]) of the HF/paired group and calculated the amount of HF diet food that should be administered to the HF/paired group (E [cal]) ($E = C*D$) on the following day.

In addition, the HF group and HF/Paired group were provided a mixture of 4% amino acids dissolved in the drinking water (all 20 naturally occurring amino acids except Gln and Asn, 19% of BCAAs in the 18 amino acids mixture as referred to their proportion in casein[13]. BCAAs concentration in "paired" drinking water is 4% × 19% = 0.76%. BCAAs (4%) were dissolved in drinking water at a leucine-isoleucine-valine ratio of 2:1:1. The total food was divided into two portions and provided at separate times (8:00 A.M. and 6:00 P.M.) to prevent starvation. A 60% HF diet was provided to the HF/paired group.

Cell experiments

Culture of primary podocytes. This procedure was conducted as previously described[28]. Glomeruli were isolated from 6- to 8-week-old male or female C57BL/6 mice, and the isolated glomeruli were plated on collagen-type-1-coated 6-well plates at 37 °C in RPMI 1640 medium supplemented with 10% FBS. After 3 days of culture, the unattached glomeruli were washed away. Podocytes were used for experiments on day 6 of culture.

Mouse podocyte cell lines. Mouse podocytes were purchased from BeNa Culture Collection Corporation. These cell lines were confirmed to be mycoplasma negative (MycoAlert Detection Kit, Lonza). Podocytes were cultured in RPMI medium with 10% FBS at 33 °C and then thermo-shifted to 37 °C for 10 d before they were used for experiments. Only passages 14 – 18 were used for experiments.

Mouse kidney pathology assessment. We used 4-μm sections from paraformaldehyde-fixed and paraffin-embedded kidneys for immunohistochemistry or immunofluorescence staining. Periodic acid-Schiff (PAS) staining was performed by using a staining kit (Solarbio, Beijing, China) according to the manufacturer's instructions. Wilm's tumor 1 (WT1) staining and oil red O staining were performed to determine the number of podocytes and lipid droplet accumulation in the kidney sections. Cell death in kidney sections was detected by a TUNEL assay following the manufacturer's protocol (Roche

Diagnostics, Mannheim, Germany). Quantitation of the staining was performed in a blinded manner. The staining was quantified using ImageJ software (NIH, Bethesda, MD, USA) and is shown as the positive area/glomerulus area or the positive number/glomerulus.

Transmission electron microscopy. Tissue blocks of approximately 5 mm^3 were collected from each kidney (including the renal cortex) and fixed in 2.5% glutaraldehyde at 4 °C. The sections were washed 3 times for 15 min each in 0.1 mol/L phosphate-buffered saline (PBS) and postfixed in 1% osmium tetroxide at room temperature for 2 h. The specimens were then dehydrated in a series of 30%, 50%, 70%, 80%, 90%, 95%, and 100% ethanol and 100% acetone. After dehydration, the sections were embedded according to standard protocols. Glomerular filtration barrier membrane (GBM) measurements and foot process width were generated from transmission electron microscopy images. Transmission electron microscopy (TEM) images were analyzed using ImageJ software. For each kidney, 20 perpendicular measurements of the GBM were taken to generate the mean GBM value.

Biochemical analysis of serum/urine samples. After fasting overnight, plasma glucose, creatinine, blood urea nitrogen (BUN), and uric acid levels were measured. Urinary albumin was measured using an immune turbidimetric method, and urinary creatinine was measured by an enzymatic method, both of which were performed on an automated analyzer.

Mouse glomeruli isolation. After anesthetization, the thorax and abdominal cavity of each mouse were exposed. A total of 4-5 ml of 1% iron oxide solution (iron (III) oxide, Sigma, 310050) in PBS was perfused through the left ventricle until the kidney turned black. The minced kidney tissues were digested in 1 mg/ml collagenase A and 100 U/ml DNase I for 30 min. The digested mixture was then passed through a 100-μm cell strainer, and the eluate was then placed on a magnet for purification of the glomeruli by magnetic reaction of the iron (III) oxide. The purity of the glomeruli in each sample was confirmed to be 95% by phase-contrast microscopy.

Immunofluorescence staining. Paraffin sections of human kidney biopsies and mouse kidneys were deparaffinized with xylene, and ethanol and 2% hydrogen peroxide in methanol were used to ablate peroxidase activity. The sections were placed in 0.1 mol/L sodium citrate buffer (pH 6.0) and then heated to 95 °C for 15 min. The sections were then blocked with 5% normal goat serum (ZSGB-BIO, China) for 1 h and incubated with primary antibodies at 4 °C overnight. The primary antibodies used included those against P-BCKDE1α (Ser 293), WT1, PP2Cm, and BDK. After washing with PBS, the sections were incubated with secondary antibodies for 1 h, and images were collected by confocal microscopy. We measured the intensities of BDK and PP2Cm (normalized to DAPI) in WT1 positive podocytes as previously reported[84], and quantified their expression per podocyte, $n > 100$ cells per group.

Crosslinking to determine PKM2 tetramers, dimers, and monomers. For cultured podocytes, we used 500 μM disuccinimidyl suberate (DSS, Thermo Scientific, #PI21658) to cross-link the proteins at 4 °C according to the manufacturer's instructions. Equal numbers of cells were lysed in 4× Bolt LDS Sample Buffer (Invitrogen, B0007) and boiled for 8 min. Samples were separated by NuPAGE Novex 4–12% Bis-Tris Gel (Invitrogen, NP0322BOX). After transfer, the membranes were incubated with 0.4% paraformaldehyde in PBS for 30 min at room temperature before they were incubated with primary PKM2 antibody at 4 °C overnight.

GTT and ITT assays. Glucose tolerance tests (GTTs) and insulin tolerance tests (ITTs) were performed as previously described[15,85]. Mice were injected intraperitoneally with human insulin (Eli Lilly at 0.75 IU/g body weight or 20% glucose at 2.0 mg/g body weight after overnight food deprivation. Blood glucose was measured 0, 15, 30, 60, 90, and 120 min after injection.

Glucose flux in mitochondria and glycolysis. Assays were conducted using an XF24 Extracellular Flux Analyzer. During the Seahorse experiments, Seahorse assay media (Sigma–Aldrich, D5030) supplemented with 1% FBS was used. No glucose, pyruvate, or glutamine was included in the assay medium during Seahorse analysis. The oxygen consumption rate (OCR) and extracellular acidification rate (ECAR) were measured using a FluxPak Mini Kit (#100867-100, Seahorse Biosciences). The data were calculated from four independent measurements obtained at 5-minute intervals at baseline and after the addition of the following compounds at working concentrations: glucose (10 mM), oligomycin (5 μM), 2-DG (100 mM), FCCP (1.5 μM), and rotenone (5 μM). For each experiment, the means from 6 replicate wells were recorded. The values are presented as the means ± SDs. The experiments were repeated five times.

[U-^{13}C6]-glucose for metabolic flux study. Podocytes were grown to 80% confluence in 10 cm plates with standard medium, and washed three times with sterile PBS, and then podocytes were cultured in 25 mM glucose or 25 mM glucose plus 3 mM BCAAs (leucine: isoleucine: valine =1:1:1) for 24 h. Following three washes with PBS, glucose was replaced with [U-^{13}C6]-glucose (Sigma) supplemented with dialyzed Fetal Bovine Serum (GIBCO), and podocytes were exposed to 25 mM [U-^{13}C6]- glucose (Sigma) or 25 mM [U-^{13}C6]-glucose (Sigma) plus 3 mM BCAAs for another 6 h, as previously reported[86,87].

Then, the extraction buffer was added, and the mixture was centrifuged. The supernatants were collected and transferred to an autosampler vial for GC/MS analysis. A Shimadzu GCMS-QP2010 Ultra was programmed with an injection temperature of 250 °C and injected with 1 μl of sample. GC oven temperature started at 110 °C for 4 min, rising to 230 °C at 3 °C/min and to 280 °C at 20 °C/min with a final hold at this temperature for 2 min. GC flow rate with helium carrier gas was 50 cm/s. The GC column used was a 20 m x 0.25 mm×0.25 mm Rxi-5ms. GC-MS interface temperature was 300 °C and (electron impact) ion source temperature was set at 200 °C, with 70 V ionization voltage. The mass spectrometer was set to scan m/z range 50-800, with 1 kV detector.

To determine ^{13}C labeling, the mass distribution for known fragments of metabolites was extracted from the appropriate chromatographic peak. These fragments contained either the whole carbon skeleton of the metabolite, or lacked the alpha carboxyl carbon, or contained only the backbone minus the side-chain[88]. For each fragment, the retrieved data comprised mass intensities for the lightest isotopomer (without any heavy isotopes, M0), and isotopomers with increasing unit mass (up to M6) relative to M0. These mass distributions were normalized by dividing by the sum of M0 to M6 and corrected for the natural abundance of heavy isotopes of the elements H, N, O, and C, using matrix-based probabilistic methods, and implemented in MATLAB. Labeling results are expressed as the average fraction of the particular compound that contains an isotopic label from the particular precursor. MATLAB Flux-8 software was used to analyze the 13 C flux ratio data and identify changes in metabolic pathways.

Quantification of BCAA in the plasma and isolated glomeruli. The quantification of BCAAs in the plasma of PP2Cm knockout mice was determined with a commercially available BCAAs detection kit (Biovision, USA) per the manufacturer's instructions, as we previously reported[48].

For the quantification of BCAAs and BCKAs in isolated glomeruli. 20 mg of isolated glomeruli was homogenized in 500 μL of precooled aqueous methanol (4:1, v/v) at 20 Hz for 1.5 min (Qiagen, Germany). The homogenate was vortexed for 1.5 min, followed by incubation at

−20 °C for 1 h to precipitate proteins and extract metabolites. After centrifugation at 14,000 g for 10 min at 4 °C, 200 µL of the supernatant was collected and dried under nitrogen gas. The residue was then redissolved in 100 µL of MeOH: H2O (1:1, v/v) for LC-MS analysis. The determination of BCAAs and BCKAs was performed on an LC-30AD UHPLC system (Shimadzu, Japan) coupled with a Qtrap 6500plus mass spectrometer (Sciex). The separation was carried out at 40 °C using an ACQUITY UPLC HSS T3 column (2.1×100 mm, 1.8 µm). The mobile phases consisted of water (A) and acetonitrile (B), both containing 0.1% formic acid. The flow rate was set at 0.4 mL/min, and the injection volume was 1 µL. The optimized gradient elution program was as follows: 0–1 min, 1% B; 1–3 min, linear gradient to 7% B; 3–6 min, linear gradient to 50% B; 6–9 min, linear gradient to 95% B; 9–12 min, 95% B. In positive ion mode, the detection of isoleucine, leucine, and valine was achieved with the following ion pairs and retention times: isoleucine (132.1 → 86.0, RT 2.2 min), leucine (132.1 → 86.0, RT 2.44 min), and valine (118.0 → 72.0, RT 1.05 min). In negative ion mode, the detection of ketoleucine (KIC), ketovaline (KIV), and ketoisoleucine (KMV) was achieved with the following ion pairs and retention times: KIC (115.1 → 70.9, RT 3.52 min), KIV (144.8 → 101.0, RT 0.98 min), KMV (129.0 → 101.0, RT 4.72 min). BCAAs and BCKAs concentrations were measured and normalized to the weight of tissue. Both instruments used in this analysis were housed in Fudan University, China.

Gene expression analysis. For gene expression analyses, total RNA from podocytes and kidney tissues was extracted using TRIzol Reagent (Invitrogen). cDNA was synthesized using a reverse transcription kit (RR047A, Takara Bio) per the manufacturer's instructions. SYBR Green-based real-time quantitative PCR was performed using an Applied Biosystems 7300 instrument. Relative mRNA expression levels were normalized to those of β-actin. All the data were analyzed using GraphPad Prism 8 software. The primer pair sequences used are listed in Table S3.

Quantification, statistics and reproducibility. Statistical analyses were performed with Prism software (GraphPad 8). Statistical significance was assessed as follows: data sets with more than two groups were analyzed with one-way ANOVA, and data sets comparing two groups were assessed with unpaired two-tailed t tests. P values < 0.05 were considered to indicate statistical significance. The data are presented as the means ± SDs. The representative experiments (Figs. 2I, J, 3C, 5A, B, D, 6A, C, D, G, H, 7D, H) were independently repeated at least 3 times with similar results.

Reporting summary

Further information on research design is available in the Nature Portfolio Reporting Summary linked to this article.

Data availability

Source data for Figs. 1–8 and Supplementary Figs. 1–9 have been provided as Source Datafiles. The raw RNA-sequencing data of podocytes have been deposited in NCBI's Gene Expression Omnibus (GEO) database under accession code GSE283568. The Non-target metabolomics data of human urine have been submitted to National Genomics Data Center database under accession code PRJCA036343 (https://ngdc.cncb.ac.cn/gsub/submit/bioproject/list). And the Non-target metabolomics data of human urine have also been provided as Supplemental Data1. The analysis in this study used standard techniques and protocols without generating new unique reagents or custom code.

References

1. Collins, A. J. et al. US renal data system 2013 annual data report. *Am. J. Kidney Dis.* **63**, A7 (2014).
2. Krolewski, A. S., Skupien, J., Rossing, P. & Warram, J. H. Fast renal decline to end-stage renal disease: an unrecognized feature of nephropathy in diabetes. *Kidney Int* **91**, 1300–1311 (2017).
3. van Zuydam, N. R. et al. A genome-wide association study of diabetic kidney disease in subjects with type 2 diabetes. *Diabetes* **67**, 1414–1427 (2018).
4. Maxwell, S. et al. Set7 methyltransferase and phenotypic switch in diabetic glomerular endothelial cells. *J. Am. Soc. Nephrol.* **35**, 733–748 (2024).
5. Kato, M. & Natarajan, R. Epigenetics and epigenomics in diabetic kidney disease and metabolic memory. *Nat. Rev. Nephrol.* **15**, 327–345 (2019).
6. Fu, Y. et al. Elevation of JAML promotes diabetic kidney disease by modulating podocyte lipid metabolism. *Cell Metab.* **32**, 1052–1062 e1058 (2020).
7. Forbes, J. M. & Thorburn, D. R. Mitochondrial dysfunction in diabetic kidney disease. *Nat. Rev. Nephrol.* **14**, 291–312 (2018).
8. Wu, H. et al. Mapping the single-cell transcriptomic response of murine diabetic kidney disease to therapies. *Cell Metab.* **34**, 1064–1078 e1066 (2022).
9. Xu, F. et al. Discovery of PRDM16-Mediated TRPA1 Induction as the Mechanism for Low Tubulo-Interstitial Fibrosis in Diabetic Kidney Disease. *Adv. Sci. (Weinh.)* **11**, e2306704 (2024).
10. Sun, J. K. et al. Protection from retinopathy and other complications in patients with type 1 diabetes of extreme duration: the joslin 50-year medalist study. *Diabetes Care* **34**, 968–974 (2011).
11. Keenan, H. A. et al. Clinical factors associated with resistance to microvascular complications in diabetic patients of extreme disease duration: the 50-year medalist study. *Diabetes Care* **30**, 1995–1997 (2007).
12. Layman, D. K. The role of leucine in weight loss diets and glucose homeostasis. *J. Nutr.* **133**, 261S–267S (2003).
13. Newgard, C. B. et al. A branched-chain amino acid-related metabolic signature that differentiates obese and lean humans and contributes to insulin resistance. *Cell Metab.* **9**, 311–326 (2009).
14. Kawaguchi, T. & Torimura, T. Branched chain amino acids: A factor for zone 3 steatosis in non-alcoholic fatty liver disease. *Hepatol. Res* **49**, 841–843 (2019).
15. Zhao, H. et al. Branched-chain amino acids exacerbate obesity-related hepatic glucose and lipid metabolic disorders via attenuating Akt2 signaling. *Diabetes* **69**, 1164–1177 (2020).
16. Zhang, F. et al. Branched chain amino acids cause liver injury in obese/diabetic mice by promoting adipocyte lipolysis and inhibiting hepatic autophagy. *EBioMedicine* **13**, 157–167 (2016).
17. Mutter, S. et al. Urinary metabolite profiling and risk of progression of diabetic nephropathy in 2670 individuals with type 1 diabetes. *Diabetologia* **65**, 140–149 (2022).
18. Azushima, K. et al. Abnormal lactate metabolism is linked to albuminuria and kidney injury in diabetic nephropathy. *Kidney Int* **104**, 1135–1149 (2023).
19. Siddiqi, F. S. & Advani, A. Endothelial-podocyte crosstalk: the missing link between endothelial dysfunction and albuminuria in diabetes. *Diabetes* **62**, 3647–3655 (2013).
20. Reidy, K., Kang, H. M., Hostetter, T. & Susztak, K. Molecular mechanisms of diabetic kidney disease. *J. Clin. Invest* **124**, 2333–2340 (2014).
21. Pagtalunan, M. E. et al. Podocyte loss and progressive glomerular injury in type II diabetes. *J. Clin. Invest* **99**, 342–348 (1997).
22. White, K. E. et al. Podocyte number in normotensive type 1 diabetic patients with albuminuria. *Diabetes* **51**, 3083–3089 (2002).
23. Wharram, B. L. et al. Podocyte depletion causes glomerulosclerosis: diphtheria toxin-induced podocyte depletion in rats expressing human diphtheria toxin receptor transgene. *J. Am. Soc. Nephrol.* **16**, 2941–2952 (2005).

24. Matsusaka, T. et al. Genetic engineering of glomerular sclerosis in the mouse via control of onset and severity of podocyte-specific injury. *J. Am. Soc. Nephrol.* **16**, 1013–1023 (2005).
25. Tomita, I. et al. SGLT2 Inhibition mediates protection from diabetic kidney disease by promoting ketone body-induced mTORC1 inhibition. *Cell Metab.* **32**, 404–419.e406 (2020).
26. White, P. J. et al. The BCKDH kinase and phosphatase integrate BCAA and lipid metabolism via regulation of ATP-citrate lyase. *Cell Metab.* **27**, 1281–1293.e1287 (2018).
27. Sun, H., Lu, G., Ren, S., Chen, J. & Wang, Y. Catabolism of branched-chain amino acids in heart failure: insights from genetic models. *Pediatr. Cardiol.* **32**, 305–310 (2011).
28. Qi, W. et al. Pyruvate kinase M2 activation may protect against the progression of diabetic glomerular pathology and mitochondrial dysfunction. *Nat. Med.* **23**, 753–762 (2017).
29. Li, H., Dixon, E. E., Wu, H. & Humphreys, B. D. Comprehensive single-cell transcriptional profiling defines shared and unique epithelial injury responses during kidney fibrosis. *Cell Metab.* **34**, 1977–1998.e1979 (2022).
30. Wilson, P. C. et al. Multimodal single cell sequencing implicates chromatin accessibility and genetic background in diabetic kidney disease progression. *Nat. Commun.* **13**, 5253 (2022).
31. Umanath, K. & Lewis, J. B. Update on diabetic nephropathy: Core curriculum 2018. *Am. J. Kidney Dis.* **71**, 884–895 (2018).
32. Laeger, T. et al. Leucine acts in the brain to suppress food intake but does not function as a physiological signal of low dietary protein. *Am. J. Physiol. Regul. Integr. Comp. Physiol.* **307**, R310–R320 (2014).
33. Eid, S. A. et al. Dietary interventions improve diabetic kidney disease, but not peripheral neuropathy, in a db/db mouse model of type 2 diabetes. *FASEB J.* **37**, e23115 (2023).
34. Luo, W. & Semenza, G. L. Emerging roles of PKM2 in cell metabolism and cancer progression. *Trends Endocrinol. Metab.* **23**, 560–566 (2012).
35. Christofk, H. R. et al. The M2 splice isoform of pyruvate kinase is important for cancer metabolism and tumour growth. *Nature* **452**, 230–233 (2008).
36. Hitosugi, T. et al. Tyrosine phosphorylation inhibits PKM2 to promote the Warburg effect and tumor growth. *Sci. Signal* **2**, ra73 (2009).
37. Yang, W. et al. ERK1/2-dependent phosphorylation and nuclear translocation of PKM2 promotes the Warburg effect. *Nat. Cell Biol.* **14**, 1295–1304 (2012).
38. Brouwers, M. Fructose 1-phosphate, an evolutionary signaling molecule of abundancy. *Trends Endocrinol. Metab.* **33**, 680–689 (2022).
39. Luo, W. et al. Pyruvate kinase M2 is a PHD3-stimulated coactivator for hypoxia-inducible factor 1. *Cell* **145**, 732–744 (2011).
40. Teske, B. F. et al. CHOP induces activating transcription factor 5 (ATF5) to trigger apoptosis in response to perturbations in protein homeostasis. *Mol. Biol. Cell* **24**, 2477–2490 (2013).
41. Tremblay, B. P. & Haynes, C. M. Mitochondrial distress call moves to the cytosol to trigger a response to stress. *Nature* **579**, 348–349 (2020).
42. Angiari, S. et al. Pharmacological activation of pyruvate kinase M2 inhibits CD4(+) T cell pathogenicity and suppresses autoimmunity. *Cell Metab.* **31**, 391–405.e398 (2020).
43. Tso, S. C. et al. Benzothiophene carboxylate derivatives as novel allosteric inhibitors of branched-chain alpha-ketoacid dehydrogenase kinase. *J. Biol. Chem.* **289**, 20583–20593 (2014).
44. Coca, S. G., Ismail-Beigi, F., Haq, N., Krumholz, H. M. & Parikh, C. R. Role of intensive glucose control in development of renal end points in type 2 diabetes mellitus: systematic review and meta-analysis intensive glucose control in type 2 diabetes. *Arch. Intern Med.* **172**, 761–769 (2012).
45. Kidney Disease: Improving global outcomes diabetes work, G KDIGO 2020 clinical practice guideline for diabetes management in chronic kidney disease. *Kidney Int* **98**, S1–S115 (2020).
46. Yoneshiro, T. et al. BCAA catabolism in brown fat controls energy homeostasis through SLC25A44. *Nature* **572**, 614–619 (2019).
47. Verkerke, A. R. P. et al. BCAA-nitrogen flux in brown fat controls metabolic health independent of thermogenesis. *Cell*, https://doi.org/10.1016/j.cell.2024.03.030 (2024).
48. Lian, K. et al. Impaired adiponectin signaling contributes to disturbed catabolism of branched-chain amino acids in diabetic mice. *Diabetes* **64**, 49–59 (2015).
49. Li, Y. et al. Branched chain amino acids exacerbate myocardial ischemia/reperfusion vulnerability via enhancing GCN2/ATF6/PPAR-alpha pathway-dependent fatty acid oxidation. *Theranostics* **10**, 5623–5640 (2020).
50. Liu, M. et al. Serum branched chain amino acids: an effective indicator of diabetic kidney disease. *Front Endocrinol. (Lausanne)* **14**, 1269633 (2023).
51. Price, S. R. et al. Mechanisms contributing to muscle-wasting in acute uremia: activation of amino acid catabolism. *J. Am. Soc. Nephrol.* **9**, 439–443 (1998).
52. Carrero, J. J. et al. Etiology of the protein-energy wasting syndrome in chronic kidney disease: A consensus statement from the international society of renal nutrition and metabolism (ISRNM). *J. Ren. Nutr.* **23**, 77–90 (2013).
53. Cano, N. J., Fouque, D. & Leverve, X. M. Application of branched-chain amino acids in human pathological states: renal failure. *J. Nutr.* **136**, 299S–307S (2006).
54. Kidney Disease: Improving Global Outcomes, C. K. D. W. G KDIGO 2024 clinical practice guideline for the evaluation and management of chronic kidney disease. *Kidney Int* **105**, S117–S314 (2024).
55. Kwan, B. et al. Metabolomic Markers of kidney function decline in patients with diabetes: Evidence from the chronic renal insufficiency cohort (CRIC) study. *Am. J. Kidney Dis.* **76**, 511–520 (2020).
56. Harper, A. E., Miller, R. H. & Block, K. P. Branched-chain amino acid metabolism. *Annu Rev. Nutr.* **4**, 409–454 (1984).
57. Liu, S., Yuan, Y., Xue, Y., Xing, C. & Zhang, B. Podocyte injury in diabetic kidney disease: a focus on mitochondrial dysfunction. *Front Cell Dev. Biol.* **10**, 832887 (2022).
58. Biswas, D., Duffley, L. & Pulinilkunnil, T. Role of branched-chain amino acid-catabolizing enzymes in intertissue signaling, metabolic remodeling, and energy homeostasis. *FASEB J.* **33**, 8711–8731 (2019).
59. Shao, D. et al. Glucose promotes cell growth by suppressing branched-chain amino acid degradation. *Nat. Commun.* **9**, 2935 (2018).
60. Standage, S. W. et al. NMR-based serum and urine metabolomic profile reveals suppression of mitochondrial pathways in experimental sepsis-associated acute kidney injury. *Am. J. Physiol. Ren. Physiol.* **320**, F984–F1000 (2021).
61. Piret, S. E. et al. Kruppel-like factor 6-mediated loss of BCAA catabolism contributes to kidney injury in mice and humans. *Proc Natl Acad Sci USA* **118**, https://doi.org/10.1073/pnas.2024414118 (2021).
62. Li, T. et al. Defective branched-chain amino acid catabolism disrupts glucose metabolism and sensitizes the heart to ischemia-reperfusion injury. *Cell Metab.* **25**, 374–385 (2017).
63. Greka, A. & Mundel, P. Cell biology and pathology of podocytes. *Annu Rev. Physiol.* **74**, 299–323 (2012).
64. Tryggvason, K., Patrakka, J. & Wartiovaara, J. Hereditary proteinuria syndromes and mechanisms of proteinuria. *N. Engl. J. Med* **354**, 1387–1401 (2006).
65. Asanuma, K. et al. Synaptopodin orchestrates actin organization and cell motility via regulation of RhoA signalling. *Nat. Cell Biol.* **8**, 485–491 (2006).

66. Perico, L., Conti, S., Benigni, A. & Remuzzi, G. Podocyte-actin dynamics in health and disease. *Nat. Rev. Nephrol.* **12**, 692–710 (2016).
67. Imasawa, T. & Rossignol, R. Podocyte energy metabolism and glomerular diseases. *Int J. Biochem Cell Biol.* **45**, 2109–2118 (2013).
68. Yuan, Q. et al. Role of pyruvate kinase M2-mediated metabolic reprogramming during podocyte differentiation. *Cell Death Dis.* **11**, 355 (2020).
69. Nakajo, A. et al. Mizoribine corrects defective nephrin biogenesis by restoring intracellular energy balance. *J. Am. Soc. Nephrol.* **18**, 2554–2564 (2007).
70. Ozawa, S. et al. Glycolysis, but not Mitochondria, responsible for intracellular ATP distribution in cortical area of podocytes. *Sci. Rep.* **5**, 18575 (2015).
71. Yan, L. J. Folic acid-induced animal model of kidney disease. *Anim. Model Exp. Med.* **4**, 329–342 (2021).
72. Ortega, A. et al. Role of parathyroid hormone-related protein in tubulointerstitial apoptosis and fibrosis after folic acid-induced nephrotoxicity. *J. Am. Soc. Nephrol.* **17**, 1594–1603 (2006).
73. Handzlik, M. K. et al. Insulin-regulated serine and lipid metabolism drive peripheral neuropathy. *Nature* **614**, 118–124 (2023).
74. Yuan, M. et al. An allostatic mechanism for M2 pyruvate kinase as an amino-acid sensor. *Biochem J.* **475**, 1821–1837 (2018).
75. Chaneton, B. et al. Serine is a natural ligand and allosteric activator of pyruvate kinase M2. *Nature* **491**, 458–462 (2012).
76. Ohoka, N., Yoshii, S., Hattori, T., Onozaki, K. & Hayashi, H. TRB3, a novel ER stress-inducible gene, is induced via ATF4-CHOP pathway and is involved in cell death. *EMBO J.* **24**, 1243–1255 (2005).
77. Cui, Y. et al. crosstalk between endoplasmic reticulum stress and oxidative stress in heat exposure-induced apoptosis is dependent on the ATF4-CHOP-CHAC1 signal pathway in IPEC-J2 cells. *J. Agric Food Chem.* **69**, 15495–15511 (2021).
78. Acevedo, A. et al. The BCKDK inhibitor BT2 is a chemical uncoupler that lowers mitochondrial ROS production and de novo lipogenesis. *J. Biol. Chem.* **300**, 105702 (2024).
79. Anastasiou, D. et al. Pyruvate kinase M2 activators promote tetramer formation and suppress tumorigenesis. *Nat. Chem. Biol.* **8**, 839–847 (2012).
80. Xiao, X. et al. Aster-B-dependent estradiol synthesis protects female mice from diet-induced obesity. *J. Clin. Invest.* **134**, https://doi.org/10.1172/JCI173002 (2024).
81. Mills, E. L. et al. Cysteine 253 of UCP1 regulates energy expenditure and sex-dependent adipose tissue inflammation. *Cell Metab.* **34**, 140–157 e148 (2022).
82. Gonzalez-Garcia, I. et al. Estradiol regulates leptin sensitivity to control feeding via hypothalamic Cited1. *Cell Metab.* **35**, 438–455.e437 (2023).
83. Mashiko, S. et al. A pair-feeding study reveals that a Y5 antagonist causes weight loss in diet-induced obese mice by modulating food intake and energy expenditure. *Mol. Pharm.* **71**, 602–608 (2007).
84. Pan, R. Y. et al. Positive feedback regulation of microglial glucose metabolism by histone H4 lysine 12 lactylation in Alzheimer's disease. *Cell Metab.* **34**, 634–648.e636 (2022).
85. Zhou, X. Y. et al. Insulin regulation of hepatic gluconeogenesis through phosphorylation of CREB-binding protein. *Nat. Med.* **10**, 633–637 (2004).
86. Metallo, C. M., Walther, J. L. & Stephanopoulos, G. Evaluation of 13C isotopic tracers for metabolic flux analysis in mammalian cells. *J. Biotechnol.* **144**, 167–174 (2009).
87. DeBerardinis, R. J. et al. Beyond aerobic glycolysis: transformed cells can engage in glutamine metabolism that exceeds the requirement for protein and nucleotide synthesis. *Proc. Natl Acad. Sci. USA* **104**, 19345–19350 (2007).
88. van Winden, W. A., Wittmann, C., Heinzle, E. & Heijnen, J. J. Correcting mass isotopomer distributions for naturally occurring isotopes. *Biotechnol. Bioeng.* **80**, 477–479 (2002).

Acknowledgements

The authors sincerely thank Xiaomeng Zhang (Department of Cardiology) and Jiangpeng Wei (Department of Gastrointestinal Surgery), both of whom are from Xijing Hospital, Fourth Military Medical University, for their helpful insights, discussions, and technological support. The authors sincerely thank the contribution of the Kidney Interactive Transcriptomics dataset, which provides the tool to query gene expression from mouse or human kidney. This work was financially supported by National Science Funds of China (grant Nos. 82100948, 82330009, 82070853, 82022004, 82370252), and was also financially supported by Shaanxi Provincial Key Research and Development Program (grant No. 2022ZDLSF01-01).

Author contributions

L.T., H.Z., W.Y., and S.W. conceived of and designed the experiments. H.Z. and D.S. performed the experiments. H.Z., D.S., S.W., Y.L., S.S., X.Z., W.T., X.D., J.L., J.X., Y.X., X.X, C.W., D.W., G.Z., X.W., L.P, H.W., F.D, P. X., F.Z., W.Y., L.T., and S.L. analyzed the data. H.Z., W.Y., and L.T. wrote the manuscript.

Competing interests

The authors declare no competing interests.

Additional information

Supplementary information The online version contains supplementary material available at https://doi.org/10.1038/s41467-025-62890-9.

Correspondence and requests for materials should be addressed to Wenjun Yan or Ling Tao.

Peer review information *Nature Communications* thanks Jianhong Ching who co-reviewed with Ming Shen Tham and Kee Voon ChuaKeizo Kanasaki, Alla Mitrofanova and the other, anonymous, reviewer for their contribution to the peer review of this work. A peer review file is available.